Fleischmann, M., et al., *Calorimetry of the palladium-deuterium-heavy water system.* J. Electroanal. Chem., 1990. **287**: p. 293.

Calorimetry of the palladium-deuterium-heavy water system

Martin Fleischmann [*], Stanley Pons, Mark W. Anderson [**], Lian Jun Li [***] and Marvin Hawkins [***]
Department of Chemistry, University of Utah, Salt Lake City, UT 84109 (U.S.A.)
(Received 21 December 1989; in revised form 28 March 1990)

ABSTRACT

It is shown that accurate values of the rates of enthalpy generation in the electrolysis of light and heavy water can be obtained from measurements in simple, single compartment Dewar type calorimeter cells. This precise evaluation of the rate of enthalpy generation relies on the non-linear regression fitting of the "black-box" model of the calorimeter to an extensive set of temperature time measurements. The method of data analysis gives a systematic underestimate of the enthalpy output and, in consequence, a slightly negative excess rate of enthalpy generation for an extensive set of blank experiments using both light and heavy water. By contrast, the electrolysis of heavy water at palladium electrodes shows a positive excess rate of enthalpy generation; this rate increases markedly with current density, reaching values of approximately 100 W cm^{-3} at approximately 1 A cm^{-2}. It is also shown that prolonged polarization of palladium cathodes in heavy water leads to bursts in the rate of enthalpy generation; the thermal output of the cells exceeds the enthalpy input (or the total energy input) to the cells by factors in excess of 40 during these bursts. The total specific energy output during the bursts as well as the total specific energy output of fully charged electrodes subjected to prolonged polarization (5-50 MJ cm^{-3}) is 10^2 - 10^3 times larger than the enthalpy of reaction of chemical processes.

INTRODUCTION

In a preliminary publication [1] (for corrections see ref. 2), we have recently reported that deuterons highly compressed by cathodic polarization in a palladium host lattice, generate enthalpy in excess of that which can be ascribed to the overall enthalpy input to the electrolytic reaction

$$2\ D_2O \rightleftharpoons 2\ D_2 + O_2$$

The magnitude of the excess enthalpy was so large (typically 1-20 W cm^{-3} of the electrode volume maintained for periods of 100 h, i.e. giving 0.36 - 7.2 MJ cm^{-3} over the measurement cycles) that it is not possible to ascribe this enthalpy release to any chemical process [1,3].

[*] To whom correspondence should be addressed. Permanent address: Department of Chemistry, University of Southampton, Southampton S09 5NH, Great Britain.
[**] Present address: Department of Chemistry, Virginia Polytechnic and State University, Blacksburg, VA 24061, U.S.A.
[***] Present address: NCFI, 390 Wakara Way, Salt Lake City, UT 84112, U.S.A.

The most surprising feature of these results (apart from the fact that nuclear processes can be induced at all in this way!) is that the enthalpy release is not due to either of the well established fusion reactions [4]

$$^{2}D + {}^{2}D \rightleftharpoons {}^{3}T(1.01\ MeV) + {}^{1}H(3.02\ MeV) \qquad (ii)$$

$$^{2}D + {}^{2}D \rightleftharpoons {}^{3}He(0.81\ MeV) + n(2.45\ MeV) \qquad (iii)$$

which have the highest (and roughly equal) cross-sections of the known reaction paths for high energy deuterons. Although low levels of tritium and, possibly, of neutrons were detected [1], the enthalpy release was evidently substantially aneutronic and atritonic. Recent work has shown that this conclusion with regard to tritium is not valid for some conditions [5-9].

These observations have received piecemeal confirmation in the time since the publication of the preliminary paper. While some research workers have confirmed the generation of excess enthalpy using a variety of calorimetric techniques (e.g. see ref. 10), some of the results being quantitatively similar to those which we reported using similar electrode materials and similar electrolysis conditions [11] and while enthalpy releases even higher than those which we achieved have been reported [12], others have found no excess enthalpy (e.g. refs. 13-16); in some cases the absence of excess enthalpy has been reported (ref. 17), even though the published data [18] could be more reasonably interpreted by assuming such an excess. Surprisingly, much of the research effort has been directed at a search for neutrons due to reaction (iii), without first attempting to verify the production of excess enthalpy. Predictably, the search for neutrons without excess enthalpy is a fruitless one. The search for tritium has proved to be more successful in some investigations (e.g. refs. 5-9), so much so that it is necessary to assume either that the branching ratio for reactions (ii) and (iii) differs greatly from unity or that completely different nuclear processes are involved.

In view of the wide disparity in the reported results and the chorus of criticism which greeted our first publication, we have completed two further measurement cycles in the intervening period. We report here the results of the calorimetric measurements and give full details of the experimental technique and methods of data analysis. The results for other types of measurements will be given elsewhere [19].

EXPERIMENTAL

Successive series of measurements carried out prior to the first publication showed that it was necessary to carry out many experiments on a substantial number of electrodes and over long periods of time (the median duration chosen for a measurement cycle was 3 months). It was necessary therefore to adopt a low cost calorimeter design; some of the reasoning underlying the choice of the single compartment Dewar-type cell design, Fig. 1, is outlined in Appendix 1.

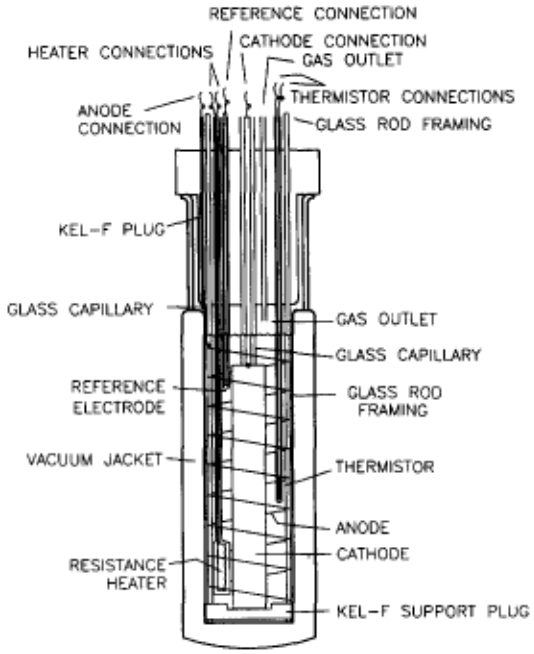

Fig. 1. Single compartment vacuum Dewar calorimeter cell.

All measurements reported in this paper were carried out with 0.1, 0.2, 0.4 and 0.8 cm diameter palladium as well as 0.1 cm diameter platinum rod electrodes. The palladium electrodes (Johnson-Matthey, PLC) came from three separate batches of material and a typical analysis is given in Table 1. These batch numbers are identified in the results given below. The palladium electrodes were welded to 0.05 cm diameter palladium lead wires and these leads (as well as those to the platinum anodes) were covered with glass shields in order to avoid any possible recombination of deuterium and oxygen in the gas head spaces of the cells. The platinum (Johnson-Matthey, 99.9%) helical anodes were tightly wound with a close spacing on cages of glass rods surrounding the cathodes. The electrodes were held in place by the deep Kel F plug and Kel F spacer at the bottom of the cell. The configuration of the anodes and cathodes assured the establishment of a uniform potential over the surfaces of the cathodes. This design assures uniform and high levels of charging of the cathodes.

TABLE 1

Typical constitutional analysis of the Johnson-Matthey palladium rods used in this work

Element	% by weight
Ag	0.0001
Al	0.0005
Au	0.003
B	0.002
Ca	0.003
Cr	0.0002
Cu	0.001
Fe	0.001
Mg	< 0.0001
Ni	0.0001
Pt	0.001
Si	< 0.0001

Temperature measurements were made with specially calibrated thermistors (Thermometrics Ultrastable Thermoprobes, ~ 10 kΩ, ±0.02% stability per year) and the cells were calibrated during each measurement cycle using a resistive heating element (Digi-key ±1% accuracy 5 × 20Ω metal film resistor chains, thermal stability better than 100 ppm/K). Connections to these components (as well as to other components (such as further thermistors and reference electrodes which were included in special cells) were made through the top Kel F plugs which also contained filling tubes and gas vents. The plugs were further sealed to the Dewars using Parafilm.

The Dewar cells were maintained in specially constructed water baths stirred with Techne Tempunit TU-16A stirrer/regulators. Since March 1989, we have maintained two or three water baths; each bath contained up to five Dewar cells so that we were able to run 8 to 15 cells simultaneously. The results presented herein are based on approximately 54 total experiments and approximately 360 cell calibrations. It was found that the bath temperature at depths greater than 0.5 cm below the surface of the water bath could be maintained to better than 0.01 K of the set temperature (which was in the vicinity of 303.15 K) provided the water surface was allowed to evaporate freely. This constant temperature was maintained throughout the bath volume. The level in each water bath was maintained constant by means of a continuous feed using a dosimeter pump connected to a second thermostatted water bath.

The minimum current used in all the experiments reported here was 200 mA and it was found that the cells could be used at currents up to 800 mA with 0.1 M LiOD as electrolyte. With 0.1 M LiOD + 0.5 M Li_2SO_4 or 1 M Li_2SO_4 electrolytes, currents up to 1600 mA could be used in view of the lower joule heating in these solutions.

The mixing history within the calorimeters for these current limits was determined using dye injection combined with video recording; radial mixing was found to be extremely rapid (time scale < 3 s) while axial mixing took place on a ~ 20 s time scale at the lowest currents used. As the thermal relaxation time of the calorimeters was ~ 1600 s (cf. eqn. A4.7), the calorimeters can be considered to be well stirred tanks. In view of the high degree of mixing and the axially uniform injection of heat, the maximum variation in temperature within the calorimeters at any

given time was found to be 0.005 K except for the region in contact with the bottom Kel F spacers where the variation reached 0.01 K. These temperature distributions were determined using cells which contained 5 thermistors which could be displaced in the radial and axial directions. Statements which have been made about the non-uniform temperature distributions in such cells [20,21] are incorrect.

All measurements reported here were made galvanostatically using HiTek Instruments Model DT2101 potentiostats connected as galvanostats. The feedback arrangement used, Fig. 2A, ensured total protection against oscillations. The galvanostat outputs were further monitored regularly to check for oscillations (none found throughout this work) and ripple content (60 and 120 Hz < 0.04 p/p of the dc currents). Measurements above 800 mA were carried out using the circuit shown in Fig. 2B; this ensured that the high degree of stabilization achievable by means of the galvanostat could be extended to much higher current levels.[*] Electrodes were charged at 64 mA cm^{-2} for times in excess of 5 diffusional relaxation times. Other current densities were then applied. Data reported here were taken after a period in excess of a further 5 diffusional relaxation times.

Heat transfer coefficients were determined daily (and for special experiments every 9 h) using galvanostats to drive the resistive heating elements. The measurement scheme adopted was as follows: the cell electrolyte volumes were replenished every 12, 24 or 48 h for experiments using currents in the range 800-1600, 400-800, and 200-400 mA respectively to a set mark and the cell temperatures were allowed to equilibrate for 3 h (> 6 thermal relaxation times); joule heating was then applied for 3 h using the resistive heaters, the input current from the galvanostats being adjusted so that the final temperature rise over the sloping baseline was ~ 2 K. The cell temperatures, cell voltages, bath temperatures and, when appropriate, the heater voltages, were monitored every 5 min using Keithley Model 199 DMM multiplexers to input data to Compaq Deskpro 386 16 MHz computers. Examples of such measurements for two different experiments at three different times are shown in Figs. 3A-C and 4A-C. The measuring circuits were maintained open except during the actual sampling periods (voltage measurements were allowed to stabilize for 2 s before sampling; thermistor resistances were allowed to stabilize for 8 s before sampling). Data were displayed in real time as well as being written to discs. Variations from these procedures for special experiments are given below.

[*] Measurements at current levels up to 25 A and using other types of calorimeter will be reported elsewhere.

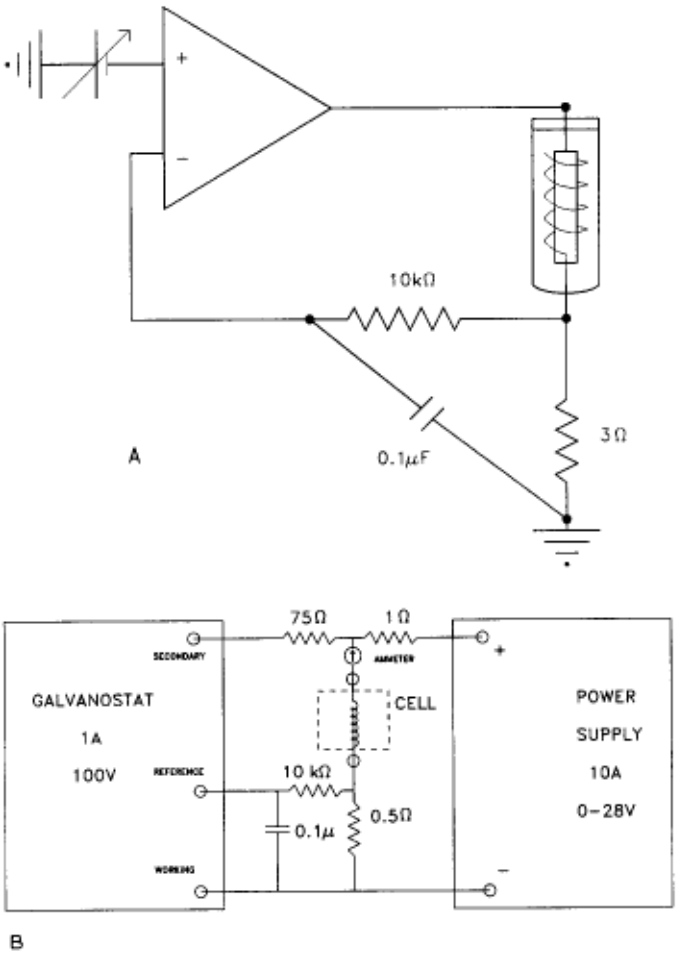

Fig. 2. (A) Schematic diagram of the feedback circuit used in this work for protection against galvanostat oscillations. (B) Schematic diagram of the circuit used in this work for high stabilization of a regulated power supply used as a high output current galvanostat.

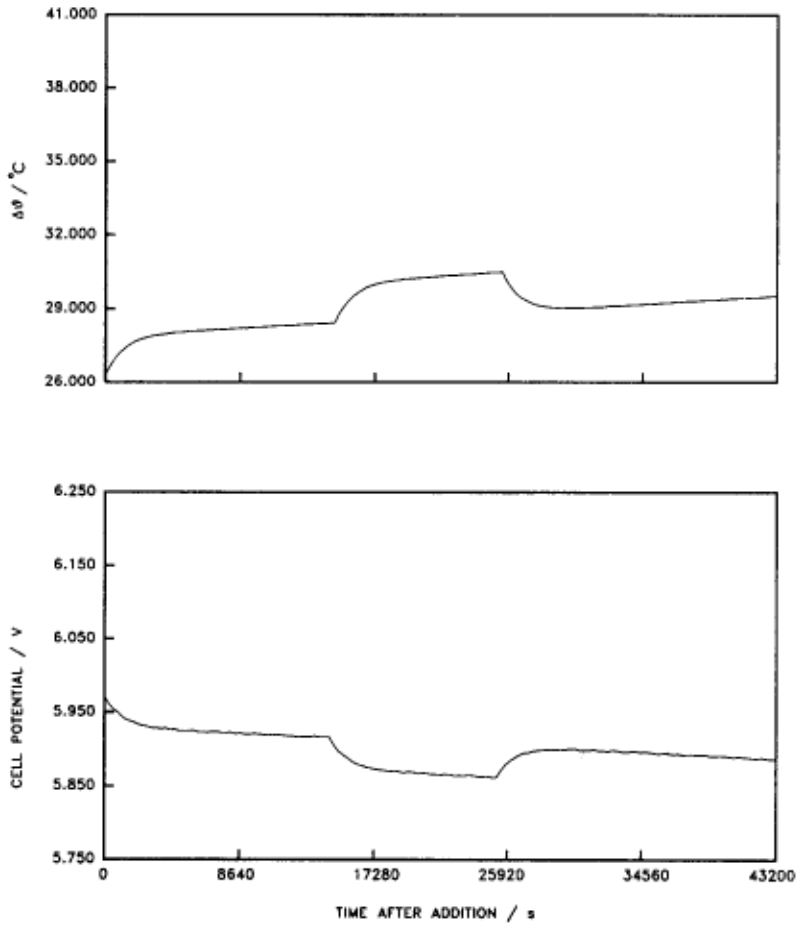

Fig. 3A. Temperature above bath vs. time (upper) and cell potential vs. time (lower) data for a 0.4 × 10 cm Pd rod in 0.1 M LiOD solution. The applied current was 800 mA, the bath temperature was 29.87ºC, and the estimated Q_f was 0.158 W. The time of the measurement (taken at the end of the calibration pulse) was approximately 0.45×10^6 s after the beginning of the experiment.

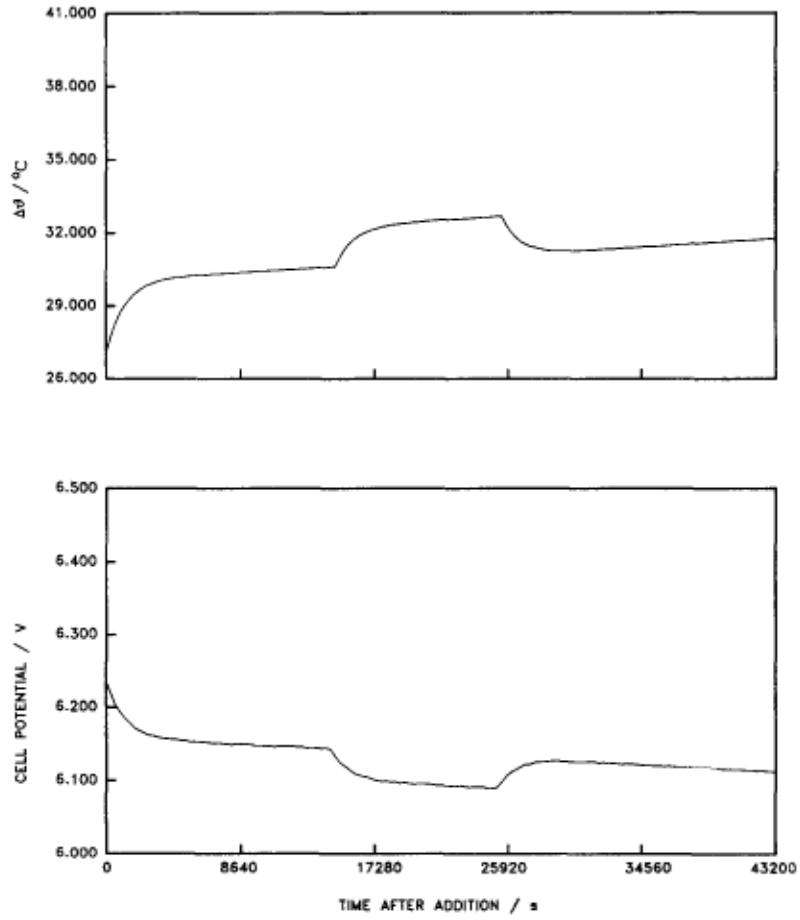

Fig. 3B. Same as Fig. 3A except time of measurement approximately 0.89×10^6 s. Estimated $Q_f = 0.178$ W.

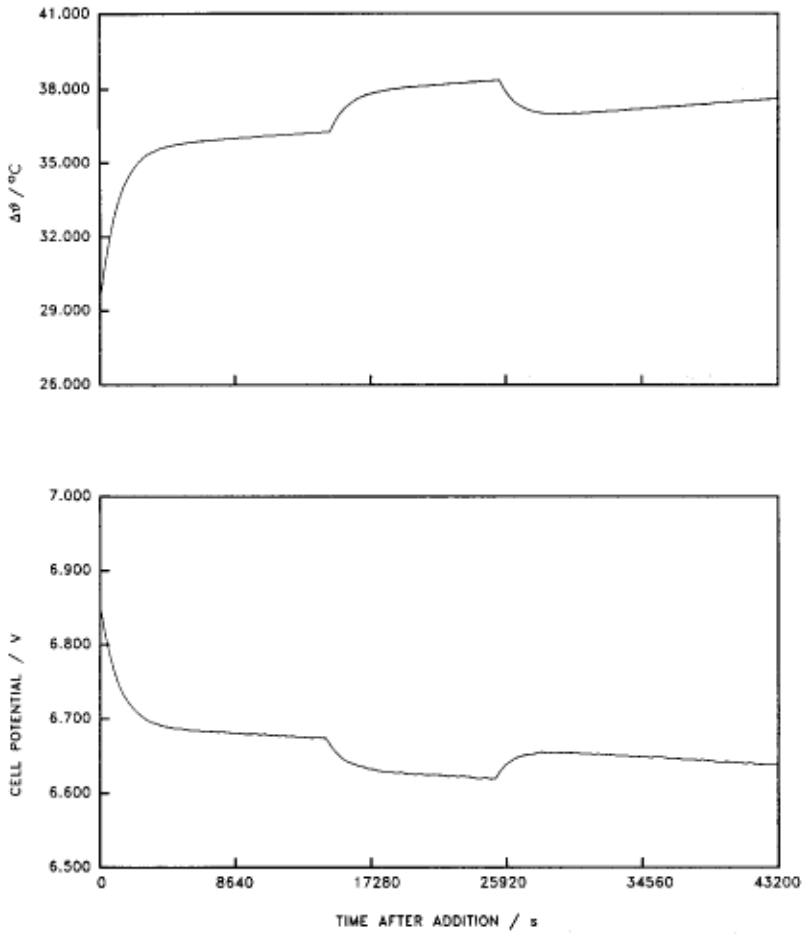

Fig. 3C. Same as Fig. 3A except time of measurement approximately 1.32x106 s. Estimated Q_f = 0.372 W.

Experiments at low and intermediate current densities were carried out using 10 cm long electrodes; for the highest current densities the electrode lengths were reduced to 1.25 cm and the spacing of the anode winding was reduced to ensure uniform current distributions; such shorter electrodes were placed at the bottom of the Dewars so as to ensure adequate stirring. Experiments were carried out using D_2O (Cambridge Isotopes) of 99.9% isotopic purity. 0.1 M LiOD was prepared by adding Li metal (A.D. Mackay, $^6Li/^7Li$ = 1/9) to D_2O; 0.1 M LiOD + 0.5 M Li_2SO_4 and 1 M Li_2SO_4 were prepared by adding dried Li_2SO_4 (Aldrich 99.99%, anhydrous, $^6Li/^7Li$ = 1/11) to 0.1 M LiOD and D_2O respectively. The light water contents of the cells were monitored by NMR and never rose above 0.5%. The ingress of H_2O may account for some of the variability in other reported results. Electrolyte withdrawn for HDO and tritium analyses (to be reported elsewhere [19]) was replaced using the appropriate electrolytes. A single batch of electrolyte was used for any given experimental series. Normal losses due to electrolysis (and evaporation at high cell temperatures) were replaced by adding D_2O.

The current efficiencies for the electrolyses according to reaction (i) were determined by measuring the combined rates of gas evolution from the cells. Surprisingly, these efficiencies were higher than 99% as was also shown by the record of D_2O additions. Such high current efficiencies have now also been reported in other work [15,22] and a number of statements made about the effects of low current efficiencies (e.g. refs. 14,23) can be seen to be in error. The high values can be understood in terms of the inhibition of D_2 oxidation at the anode by Pt-oxide

formation and by the extensive degassing of the oxygen content of the electrolyte in the cathode region by the D_2 evolution. These high current efficiencies greatly simplify the analyses of the experimental data (see Appendix 3).

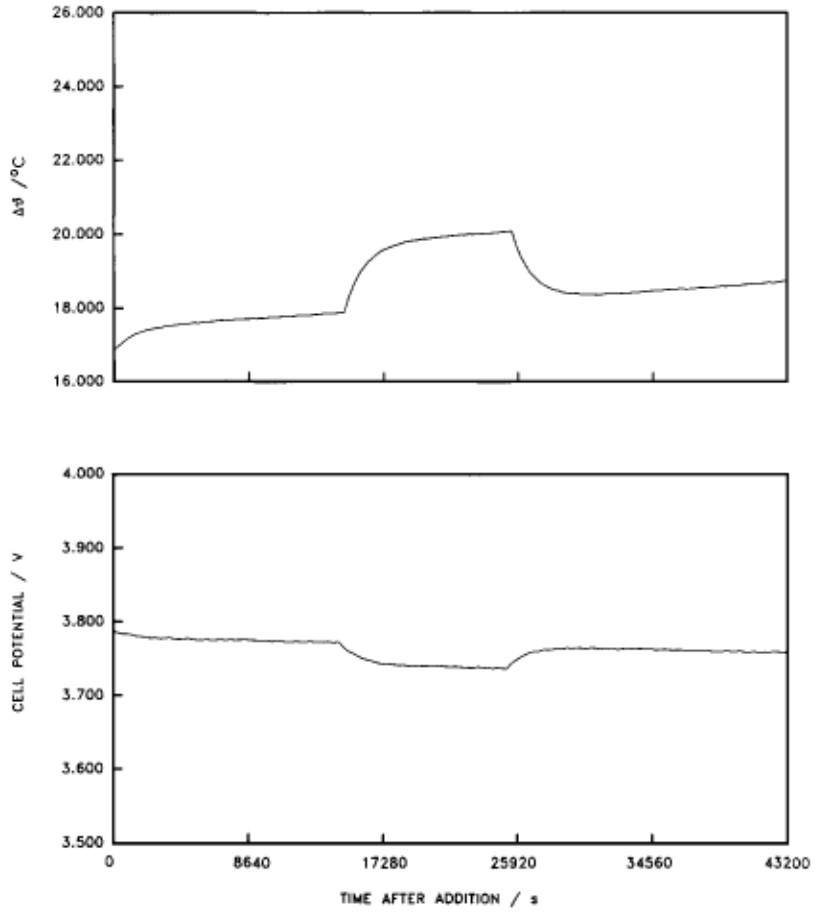

Fig. 4A. Temperature above bath vs. time and cell potential vs. time data for a 0.2 × 10 cm Pd rod in 0.1 M LiOD solution. The applied current was 800 mA, the bath temperature was 29.90°C, and the estimated Q_f was 0.736 W. The time of the measurement (taken at the end of the calibration pulse) was approximately 0.28 × 10^6 s after the beginning of the experiment.

DATA EVALUATION AND ERROR ANALYSIS

It is shown in Appendix 3 that the differential equation governing the temporal evolution of the temperature ϑ is given by eqn. (A3.9). The long-time limits of the algebraic solutions (eqns. A4.9 and A4.12) of the linearized equation (A4.2) show that the heat transfer coefficient to be used in the calculation of the total heat transfer from the cell includes the term $\psi I / \vartheta^\circ$ due to changes in the cell potential with time (see eqn. A3.10). This result would not be expected from the heat balance at a single point but would in fact be predicted from the argument outlined in Appendix 2; it emphasizes the need to fit the whole of the $\vartheta - t$ transient predicted from the inhomogeneous, non-linear differential equation representing the "black box" to the experimental data in order to obtain accurate values of the parameters of the "black box" (see below).

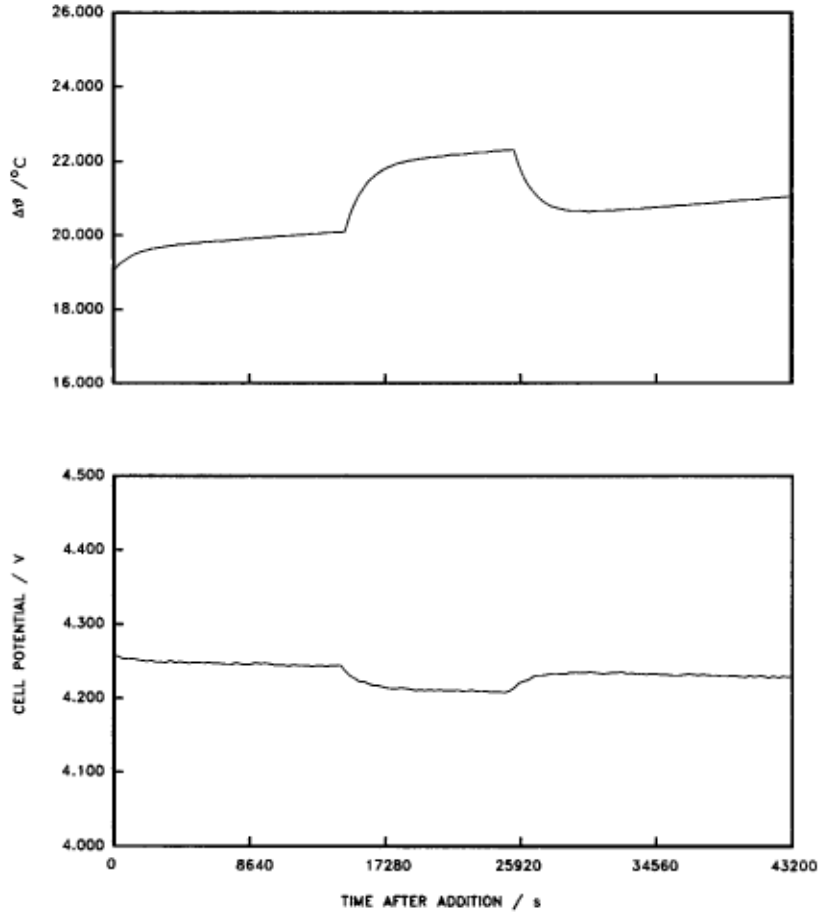

Fig. 4B. Same as Fig. 4A except time of measurement approximately 0.54×10^6 s. Estimated Q_f = 0.888 W.

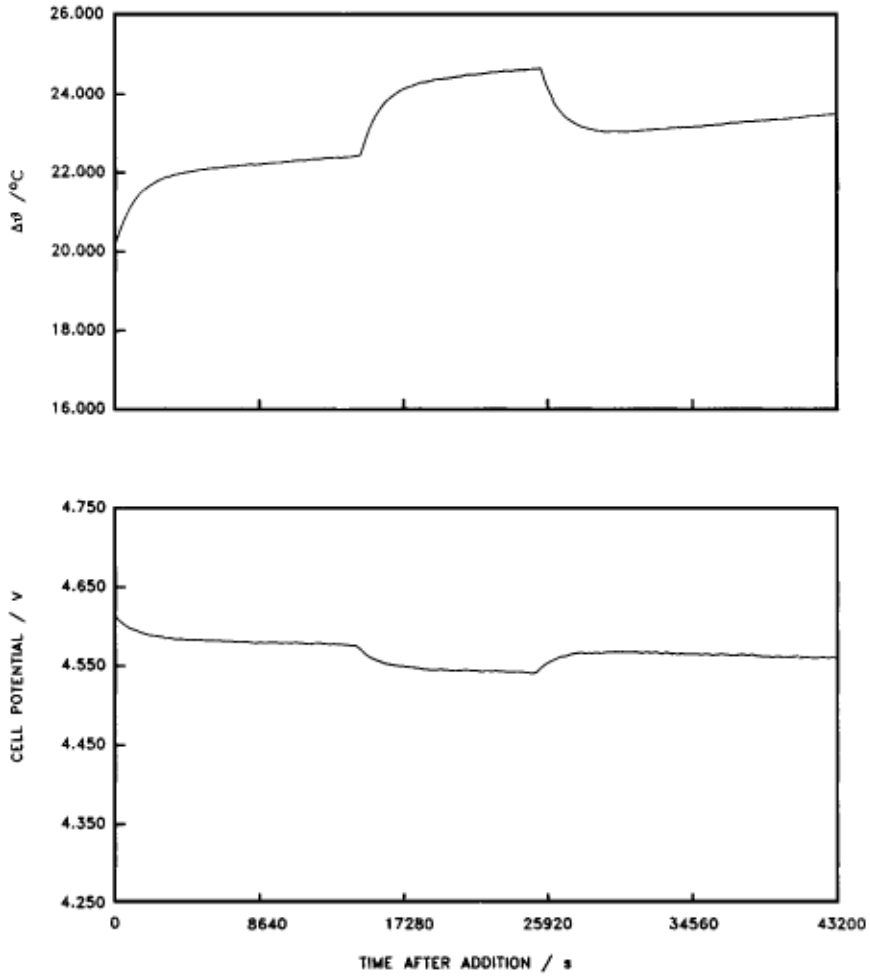

Fig. 4C. Same as Fig. 4A except time of measurement approximately 1.32×10^6 s. Estimated $Q_f = 1.534$ W.

In order to avoid the approximations inherent in using the linearization (A2.13) we have adopted the approximation (A2.9) in which the linear heat transfer term due to conduction is included in the quartic radiative term by defining a modified radiative heat transfer coefficient. As is shown in Appendix 2, any other term linear in ϑ can be similarly included in the heat transfer coefficient so that the term $\psi I \Delta \vartheta' / \vartheta^\circ$ in eqn. (A3.11) can be accounted for in this way. Accordingly we use eqns. (A2.9) and (A2.10) to obtain the approximate values of the heat transfer coefficients and rates of heat transfer rather than the linear terms (A4.9) and (A4.12). This procedure has the advantage of minimizing the errors due to temperature measurements (predicted random errors ~ 0.05%) so that the errors are dominated by that of the joule heat input ΔQ (~ 0.1%).

The prediction is borne out by the experimental measurements. Figure 5A illustrates a set of calibration cycles, and Fig. 5B shows a set of $\vartheta - t$ plots taken at different times for an 0.1 × 10 cm Pd electrode both for the temperature at the end of the resistive heating period and for the corresponding times for the sloping base lines. These lower values were derived by fitting a straight line through the measurements excluding those for the heating cycles and all points within 6 thermal relaxation times of the conclusion of these cycles. The derived heat transfer coefficients show considerable scatter, Fig. 5C, which is systematic rather than random. This

scatter must therefore be due to variations in the levels of the electrolyte following make-up after each 48 h period. Superposition of the heat transfer coefficient plots at the point 27 h after make up shows that the standard deviation of the remaining 132 measurements of the heat transfer coefficients (at 9, 18, 36 and 45 h after make up) is 0.155% for 33 separate series of measurements, Fig. 5D. (This systematic variation in the heat transfer coefficients with time and with the particular experimental sequence following the addition of D_2O shows that an evaluation of the excess enthalpy must be carried out only during or immediately following the evaluation of the heat transfer coefficient. The accurate evaluation of the heat output from the cells independent of any assumption is described below.) The validity of the procedure is further illustrated by the tests given in Table 2. In these tests, various thermal inputs were applied to the resistive heater and the heat transfer coefficient was then determined by perturbing this input. As can be seen, the thermal inputs can be accurately recovered by using the heat transfer coefficient derived from the perturbation.

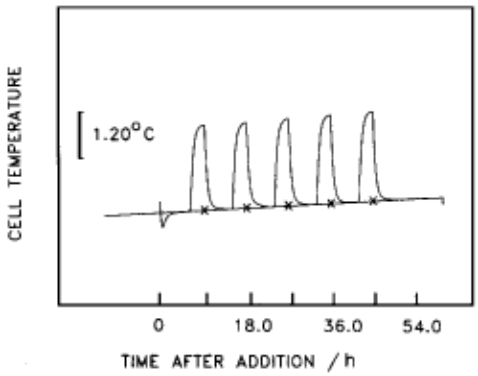

Fig. 5A. Typical set of heat flow calibration cycles made at 9, 18, 27, 36, and 45 h after addition of D_2O (0.1 × 10 cm Pd electrode in 0.1 M LiOD). Current density 64 mA cm^{-2}. (×) Baseline calculated using the information derived from Fig. 6.

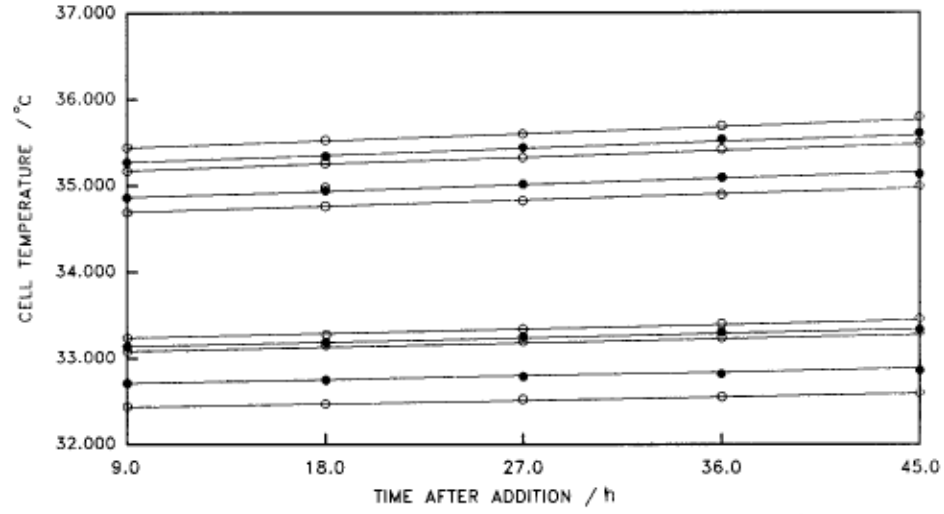

Fig. 5B. Several sets of ϑ vs. *t* data showing sloping baselines. Data points taken at end of calibration heater cycle (upper points) and at points directly below this and on a line drawn through the measurements excluding the thermal cycles and all points within 6 thermal relaxation times of the conclusion of these cycles (lower points) (see Fig. A4.1). Error in temperature measurement < 0.01 K. Current density 64 mA cm^{-2}.

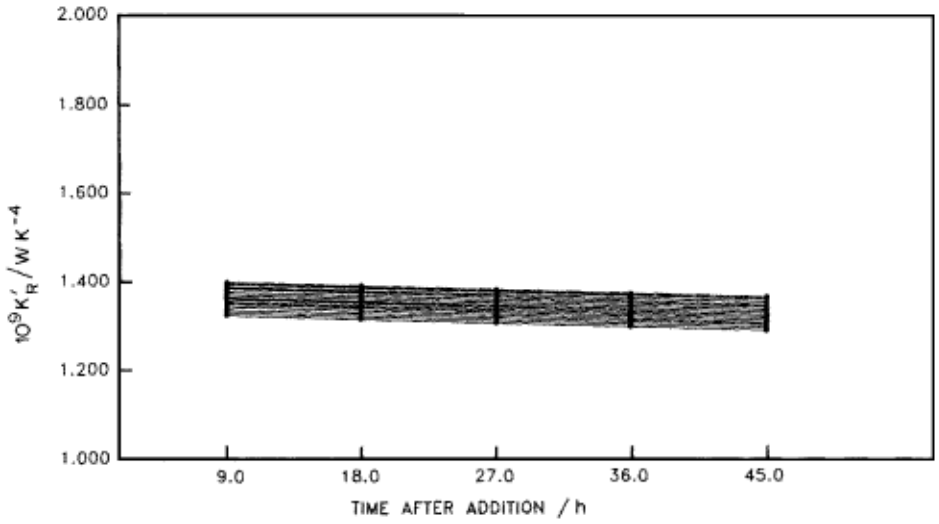

Fig. 5C. Derived heat transfer coefficients for 14 calibration cycles as a function of time after addition of D_2O

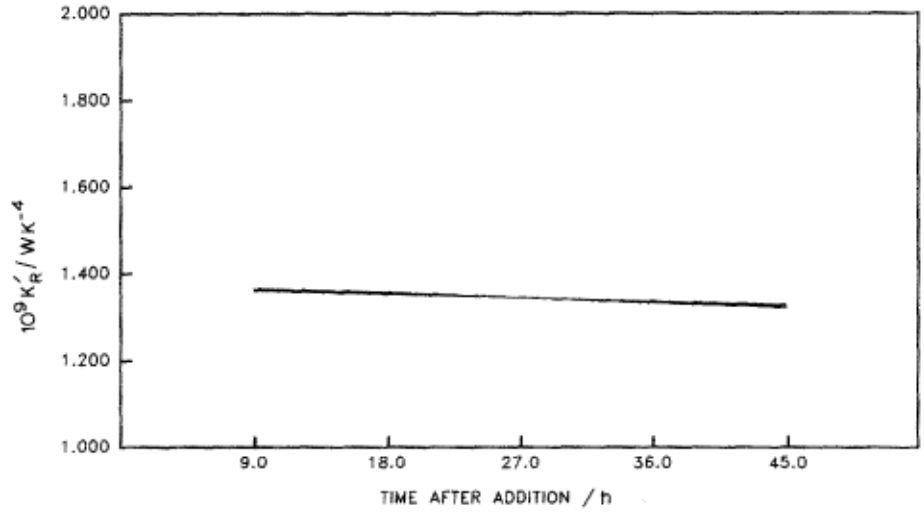

Fig. 5D. 165 derived heat transfer coefficients for 33 sets of calibration cycles for a typical cell. The individual sets have been superimposed at the 27 hour calibration point to demonstrate the precision (σ_R = 0.155%) in determining the actual coefficient at the remaining points.

TABLE 2

Heat recovery using a heat transfer coefficient determined by applying a calibration heat pulse to a test cell which is initially at a steady temperature (Column 2) and which then rises to a new steady temperature (Column 3)

Trial No.	Minimum Temperature/°C	Maximum temperature/°C	*Q* Applied /W	($Q_{Appl.}$-$Q_{Calc.}$) using k_R/W	Absolute relative error using k_R/%
1a	32.75	35.46	0.347	0.004	1.039
1b	32.74	35.46	0.347	0.001	0.303
2a	35.46	38.19	0.703	-0.004	0.587
2b	35.46	38.19	0.703	-0.003	0.410
3a	38.21	40.92	1.068	0.005	0.490
3b	38.17	40.92	1.068	-0.016	1.454
4a	40.81	43.29	1.422	0.016	1.149
4b	40.83	43.29	1.427	0.005	0.315
5a	43.20	45.48	1.759	0.006	0.325
5b	43.26	45.48	1.766	0.017	0.981
6a	45.71	48.77	2.118	0.001	0.024
6b	45.66	48.77	2.112	-0.008	0.391
7a	48.68	51.27	2.554	-0.003	0.117
7b	48.65	51.27	2.545	0.029	1.128
8a	51.01	53.37	2.906	-0.031	1.074
8b	51.05	53.37	2.909	-0.004	0.152
9a	53.38	55.30	3.264	0.010	0.297
9b	53.39	55.30	3.265	0.010	0.302

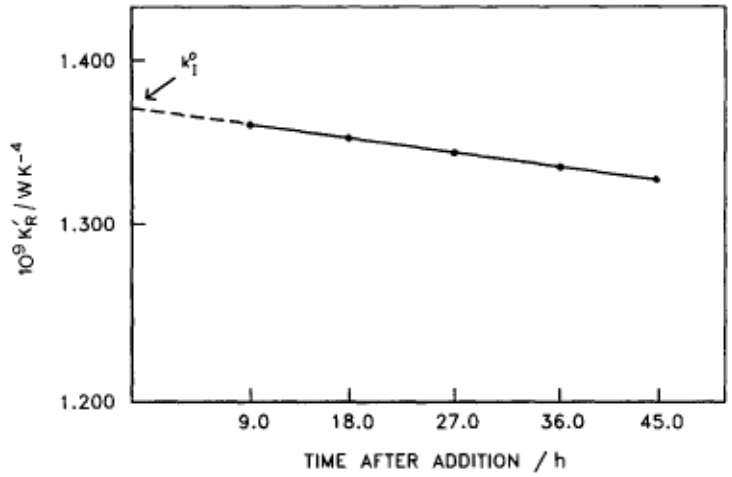

Fig. 6. Variation of the heat transfer coefficient with time for a typical cell. The slope is $(1 + \lambda)I/2\,FM$ °.

The variation of the heat transfer coefficient with time during one measurement cycle is illustrated in Fig. 6 and the slope of this plot is given by $(1 + \lambda)\, I/2\, FM$, see eqn. (A3.3). This parameter also determines the slope of the base line of the $\Delta\vartheta - t$ plot, eqn. (A4.9), Fig. 5A. It can be seen that the predicted slope is indeed close to the observed value so that the "black-box" model of Appendix 3 evidently gives an accurate representation of the -t dependencies. Nevertheless, the values of the parameters derived using this analysis are clearly approximate. A rigorous fitting of the "black box" model to the experimental data can be achieved by using the non-linear regression procedure outlined in Appendix 5 and this also gives a rigorous estimate of

the errors of all the parameters. This fitting procedure has the advantage that the whole of the $\vartheta - t$ dependencies are used in deriving the parameters of the "black box" model, including the highly structured relaxation regions following the application and removal of the resistive heating calibration term, ΔQ. It will be apparent that even better levels of accuracy could be achieved by using more highly structured $\vartheta - t$ profiles than those which have been employed in this work; the simple single calibration technique has been used in this investigation since it has been found that the accuracy of the measurement of the enthalpy output from the cell using this technique is comparable to the accuracy of the measurement of the electrical input energy (see below). Furthermore, the fitting of the "black box" model to the experimental data is independent of the level of electrolyte in the cells. It has been found that the errors in the term $[(E_{cell} - E_{thermoneutral,bath})I + Q_t]$ are dominated by the relative errors in β_1 ($\approx 0.1\%$) the errors in β_5 ($\approx 0.01\%$) being small in comparison. The errors in the total heat output of the cell are therefore in the range 0.1 to 10 mW depending on the joule output enthalpy. The error in Q_f is then increased from this value by the error in Q_{input}, which in our experiments has been dominated by the term $Q_{input}\Delta I / I$ ($\Delta I / I \approx 0.1\%$ at all current densities) which again is in the range 0.1 to 10 mW depending on the current density and electrode dimensions. The errors in the specific values of Q_f listed in Tables 3 and 4 have been derived in this way.

Figure 7A illustrates the closeness of fit which can be achieved in this way while Figs. 7B, C, D, and E illustrate the sensitivity of the analyses to the variations in the key parameters. These figures and Table 2 indicate the reasoning which underlies the statements concerning the error limits which we have repeatedly made about the measurements contained in the preliminary publication, namely, that the excess enthalpy can be determined with calorimeters of this type to within 1 mW or 1% of the enthalpy inputs whichever is the greater [1] (see also Appendix 2).

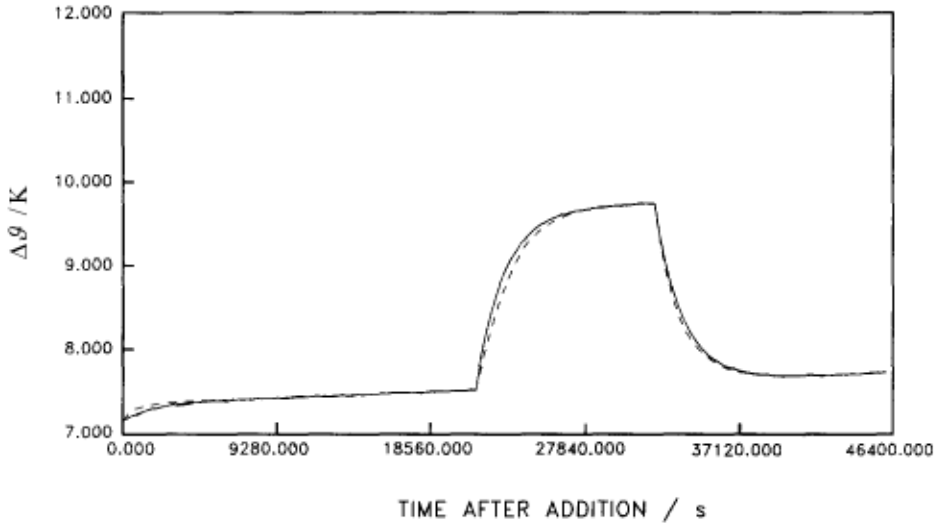

Fig. 7A. Closeness of fit of the "black box" model to experimental data (0.2 × 10 cm Pd rod in 0.1 M LiOD). (— — —) Fit using estimated values of the parameters and forward integration to force the fit at the starting point (t = 0), the point of application of the calibration heater pulse, the point of the end of the calibration heater pulse, and at the end of the experiment. (———) (here nearly coincident with the experimental data) is the fit obtained by the non-linear regression technique described in Appendix 5).

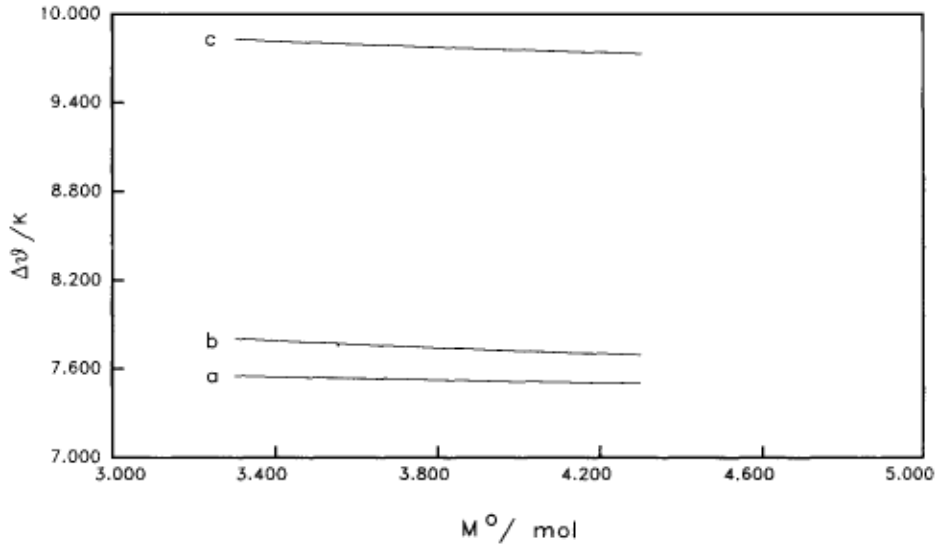

Fig. 7B. Sensitivity of the temperature A for the experiment in Fig. 3A to variation in the heavy water equivalent parameter of the cell at (a) the temperature at the time of the start of the calibration heater pulse, (b) the temperature at the end of the experimental cycle, and (c) the temperature at the end of the calibration heater pulse.

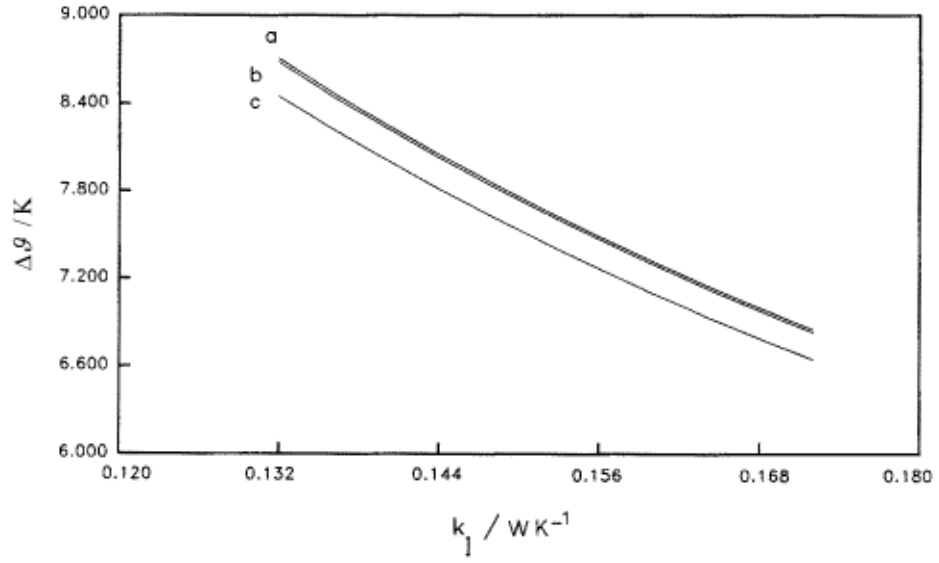

Fig. 7C. Sensitivity of the temperature $\Delta\vartheta$ for the experiment in Fig. 3A to variation in the heat transfer coefficient parameter of the cell at (a) the temperature at the time of the start of the calibration heater pulse, (b) the temperature at the end of the experimental cycle, and (c) the temperature at the end of the calibration heater pulse.

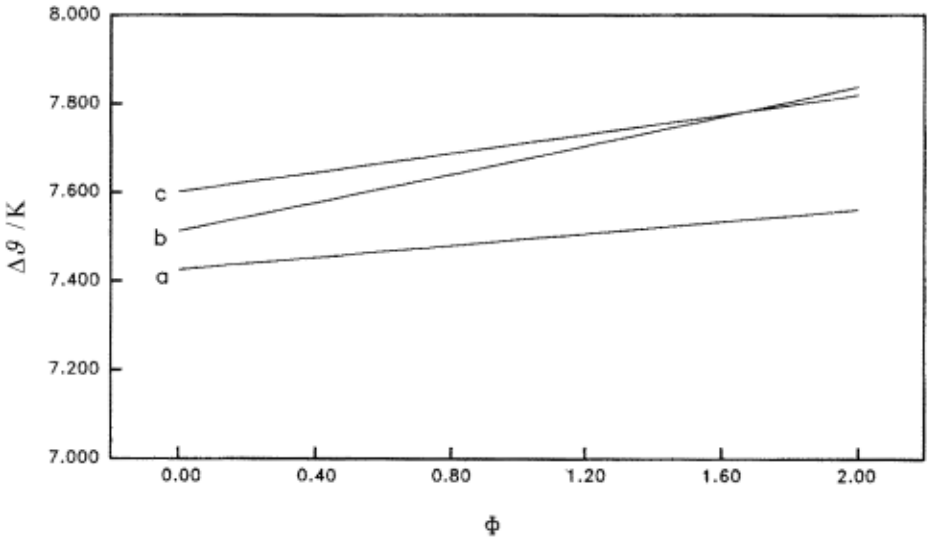

Fig. 7D. Sensitivity of the temperature $\Delta\vartheta$ for the experiment in Fig. 3A to variation in the Φ parameter of the cell at (a) the temperature at the time of the start of the calibration heater pulse, (b) the temperature at the end of the experimental cycle, and (c) the temperature at the end of the calibration heater pulse.

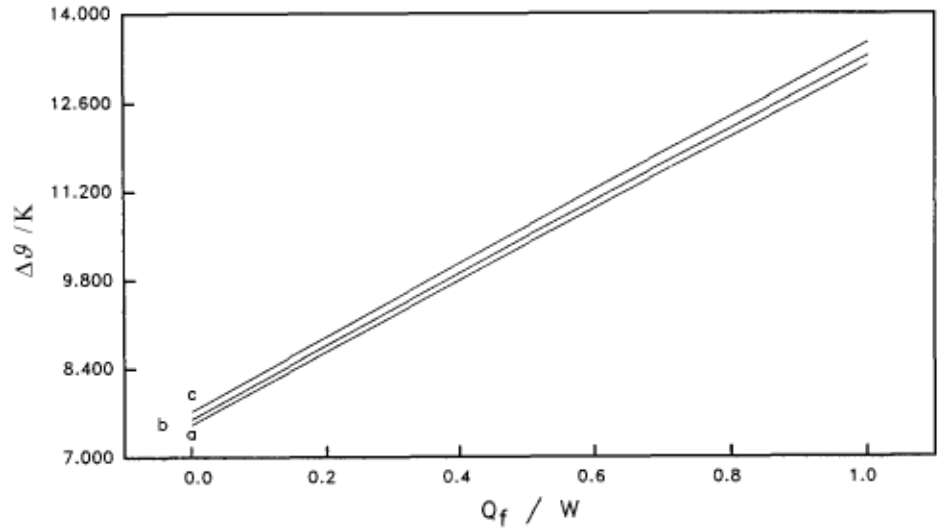

Fig. 7E. Sensitivity of the temperature $\Delta\vartheta$ for the experiment in Fig. 3A to variation in the excess enthalpy parameter of the cell at (a) the temperature at the time of the start of the calibration heater pulse, (b) the temperature at the end of the experimental cycle, and (c) the temperature at the end of the calibration heater pulse.

RESULTS

Excess enthalpy generation using Pd-rod electrodes in D_2O solutions

A summary of the results obtained using 0.1, 0.2 and 0.4 cm diameter rod electrodes is given in Table 3 while the relevant results for the preliminary publication are summarized in Table A6.1. Table 3 lists the times elapsed from the start of any particular experiment, the current density, the cell voltage, the enthalpy input, the excess enthalpy Q_f, and the excess enthalpy per

unit volume. The derived values in the Table were obtained by both the approximate method of data analysis and by the exact fitting procedure outlined in Appendix 5; error estimates are confined to the data derived by the latter method. Data are given for the three electrolytes used and the batch numbers of the particular electrodes are indicated. The measurements were made, as far as possible, when a steady state of excess enthalpy generation had been reached. However, this was not possible for some electrodes at the highest current densities used since the cells were frequently driven to the boiling point. The values given for these cases apply to the times just prior to the rapid increases in cell temperature (see section on Enthalpy Bursts).

TABLE 3

Excess enthalpy observed for 0.1, 0.2, and 0.4 cm diameter palladium rods as a function of current density, time elapsed since start of experiment, electrolyte composition, and electrode batch

Rod dia. /cm	Batch[a] and electrolyte[b]	Current density / mA cm^{-2}	10^{-6} Time /s	E_{cell} /V	Q_{input} /W	Q_{excess} /W	Approximate specific Q_{excess} /W cm^{-3}	Specific Q_{excess} from regression analysis W cm^{-3}	
0.1*	3,8,	64	6.86	2.811	0.032	0.001	0.140	0.1442	±0.0002
0.1	2,b,	128	3.88	4.000	0.984	0.160	2.04	2.043	±0.003
0.1*	3, a,	128	7.72	3.325	0.089	0.005	0.486	0.5131	±0.0006
0.1	2, b,	256	3.97	5.201	2.93	0.313	3.99	4.078	±0.007
0.1	2, b,	512	4.06	6.085	7.27	1.05	13.4	13.77	±0.02
0.1*	3,b,	1024	5.38	11.640	4.04	1.03	105	112.8	±0.1
0.2	3, a,	64	0.51	4.780	1.30	0.006	0.019	0.021	±0.001
0.2	3,c,	64	2.40	3.930	0.956	0.024	0.077	0.077	±0.001
0.2	3, b,	128	2.50	8.438	5.52	1.65	5.25	5.68	±0.01
0.2	3, a,	128	8.39	4.044	0.250	0.028	0.713	0.714	±0.001
0.2*	3,c,	256	4.92	6.032	0.898	0.056	1.42	1.498	±0.002
0.2*	3,c,	512	5.98	9.042	3.00	0.603	15.3	16.03	±0.01
0.2*	3, a,	1024	6.81	7.953	5.13	2.80	71.2	75.42	±0.08
0.4	2,b,	64	1.70	5.419	3.10	0.263	0.209	0.214	±0.003
0.4**	2.b.	64	7.44	4.745	2.24	0.117	0.106	0.145	±0.002
0.4*	2,c,	64	9.57	3.519	0.198	0.0005	0.002	0.0023	±0.0002
0.4	2,b,	128	5.92	6.852	8.50	1.05	0.84	0.842	±0.009
0.4*	2, b,	256	7.94	7.502	2.38	0.311	1.98	1.999	±0.003
0.4*	2,b,	512	8.12	10.580	7.23	1.65	10.5	11.09	±0.02

[a] All rod lengths 10 cm or * 1.25 cm or ** 8.75 cm.

[b] a: 0.50 M Li_2SO_4; b: 0.1 M LiOD; c: 0.1 M LiOD + 0.45 M Li_2SO_4. All measurements were made in the same batch of D_2O of 99.9% isotopic purity. All measurements in (a) or (c) have been made since March 1989.

TABLE 4

Results for blank experiments on platinum and palladium rods as a function of current density, time elapsed since the start of experiment, and electrolyte composition

Rod dia. [a] /cm	Batch and electrolyte [c]	Current density /mA cm^{-2}	10^{-6} Time /s	E_{cell} /V	Q_{input} /W	Q_{excess} /W	Approximate specific Q_{excess} /W cm^{-3}	Specific Q_{excess} from regression analysis W cm^{-3}	
Palladium electrodes									
0.1	2, a	32	11.32	3.605	0.212	-.001	-0.009	-0.0097	±0.0002
0.1	2, a	64	0.92	3.873	0.479	-.001	-0.014	-0.0165	±0.0005
0.1	2, a	128	3.04	5.186	1.482	-.001	-0.001	-0.001	±0.001
0.1	2, a	256	3.96	8.894	5.931	-.001	-0.007	-0.008	±0.006
0.1 [c]	2, a	512	5.40	11.29	15.70	-.001	-0.008	-0.01	±0.02
	b	0.8	3.00	2.604	1.458	-.001	-0.000		
0.8	1,b	8	1.22	3.365	0.365	-.001	-0.000	-0.001	±0.004
0.8	2,b	8	1.31	3.527	0.397	-.003	-0.000	-0.0006	±0.0003
Platinum electrodes									
0.1	b	64	1.02	3.800	0.452	0.000	0.000	-0.0007	±0.0004
0.1	b	64	2.06	4.138	0.520	-.001	-0.008	-0.0094	±0.0005
0.1	b	256	1.28	6.218	3.742	-.001	-0.028	-0.032	±0.004
0.1	a	64	3.01	4.602	0.624	-.002	-0.023	-0.0232	±0.0006
0.1	a	64	3.35	4.821	0.668	-.003	-0.038	-0.0392	±0.0006
0.1	a	512	10.25	12.02	16.86	-.001	-0.007	-0.01	±0.02

[a] All rod lengths 10 cm.
[b] a: 0.1 M LiOH; b: 0.1 M LiOD. All measurements in D_2O were made in the same batch as that used in the experiments in Table 3.
[c] Palladium sheet electrode 8×8×0.2 cm.

The values of the rates of excess enthalpy generation listed in Table 3 are lower limits because both the method of calculation (see Appendix 2) and the neglect of the latent heat of evaporation lead to an underestimate of Q_f. There is a further factor which leads to an additional underestimate of Q_f: the dissolution of D in the electrodes is exothermic and consequently the sloping base line causes a decrease in the solubility with time and therefore an absorption of heat. This factor is difficult to quantify since the deuterium content of the lattice will not be in equilibrium at any given cell temperature. We have therefore neglected all factors which would give small positive corrections to the derived values of the excess enthalpies. Of the three corrections listed above, that due to the systematic underestimate of the heat output from the cell is most significant. Estimates of the heat transfer coefficient based on eqn. (A2.9) and the methods of Appendices 4 and 5 are $k_R \cong 1.5\times10^{-9}$ W K^{-4} whereas the values calculated from the Stefan-Boltzmann coefficient are ~ 7.37 × 10^{-10} W K^{-4}; these values are increased to ~ 8.5 × 10^{-10} W K^{-4} by the inclusion of the term due to the effects of the changes in cell potential caused by changes in cell temperature. The correction factor for any particular cell temperature can then be obtained from Table A2.1.

Blank experiments

Table 4 lists the results of a variety of blank experiments: measurements with Pd electrodes in light water, with Pt electrodes in light and heavy water and measurements with 0.8 cm diameter Pd electrodes in heavy water. It can be seen that most of these experiments give small negative values for the excess enthalpy. These negative values are expected for systems giving a thermal balance according to the electrolytic reaction (i) or the corresponding reaction for light water

since both the method of calculation and the neglect of the enthalpy output from the cell due to evaporation lead to an underestimate of the heat flows from the cells (see above) [*]

Time dependence of the phenomena:"bursts" in enthalpy

Figures 8A and B are examples of the temperature-time and the associated potential-time plots in experiments which show marked increases in the heat outputs while Figs. 9A and B give the derived rates of the specific excess enthalpy release. Figures 10A and B give the time dependence of the total specific excess enthalpies for the corresponding sections of experimental data. A number of important conclusions follow from these time dependences: in the first place, the rates of excess enthalpy generation increase slowly with time; secondly, bursts in the production of excess enthalpy are superimposed on the slowly increasing or steady state enthalpy generation and these bursts occur at unpredictable times and are of unpredictable duration; following such bursts the excess enthalpy production returns to a baseline value which can be higher than just prior to the initiation of the burst; thirdly, we have found that cells are frequently driven to the boiling point, e.g. see Fig. 11. The rate of enthalpy production must become extremely large under these conditions since the dominant mode of heat transfer is now the latent heat of evaporation (see Appendix 3). It is not possible, however, at this stage to make a quantitative estimate of the heat output since the cells and instrumentation are unsuitable for making estimates under these conditions. It should also be noted that, although the cell potential initially decreases (in common to the situation for the bursts) there is usually a change to an increase of the potential with time when cells are driven to the boiling point probably due to the loss of electrolyte in spray leaving the cells.

[*] Much of this information was available at the time of the publication of the preliminary paper and at the time of submission of a letter to Nature (ref. 4 of ref. 1). The information was neither requested by the referees of the paper submitted to Nature, nor by the Editor. Although this was pointed out to the Editor of Nature, he refused to publish a letter from us asking Nature to retract the accusations made in his editorial of 27 April 1989 (J. Maddox, Nature, 338 (1989) 701).

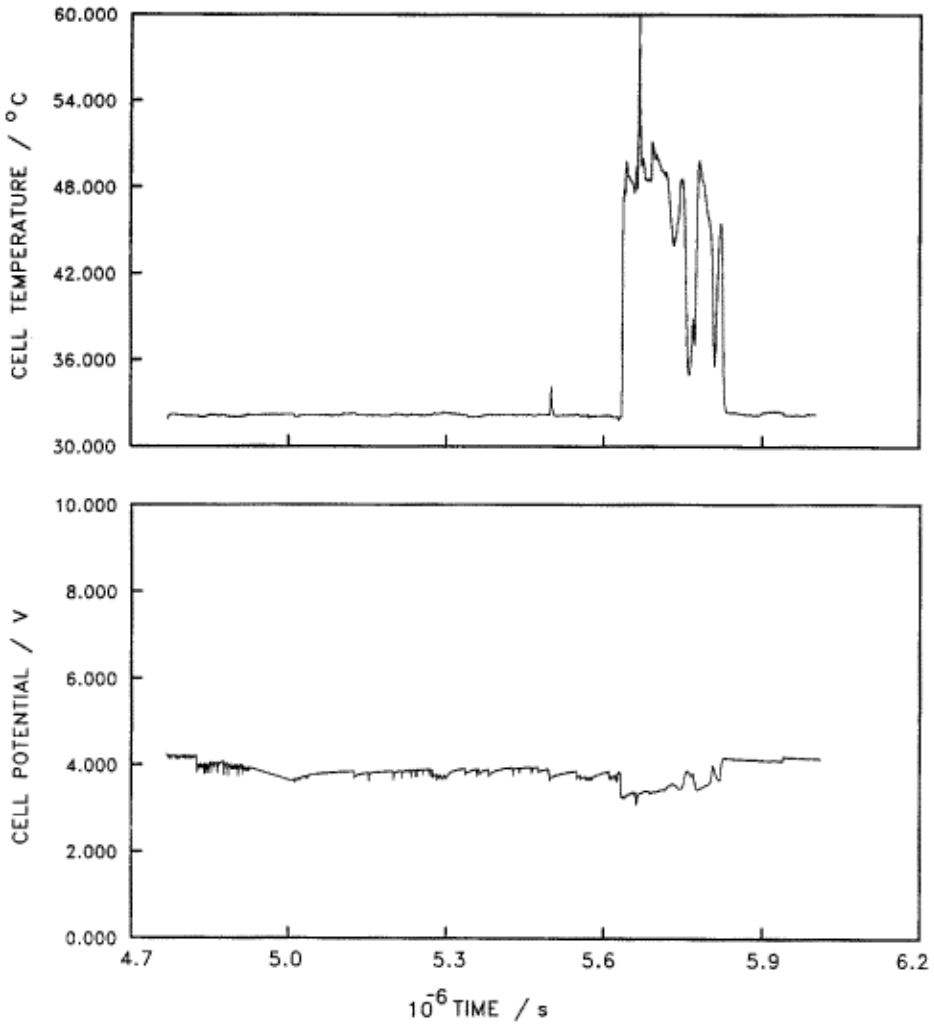

Fig. 8A. Cell temperature vs. time (upper) and cell potential vs. time (lower) plots for a 0.4 × 1.25 cm Pd rod electrode in 0.1 M LiOD solution. Current density 64 mA cm^{-2}, bath temperature 29.87ºC.

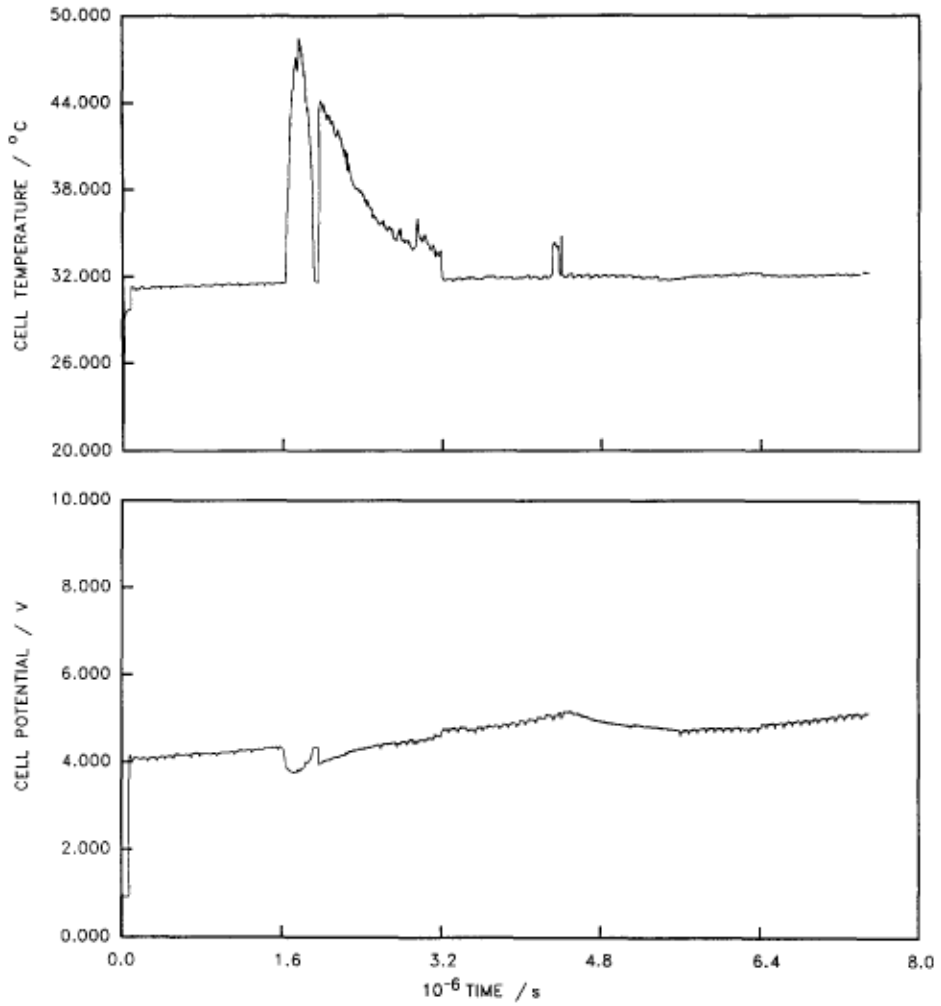

Fig. 8B. Cell temperature vs. time (upper) and cell potential vs. time (lower) plots for a 0.4 × 1.25 cm Pd rod electrode in 0.1 M LiOD solution. Current density 64 mA cm^{-2}, bath temperature 29.87ºC. This is a different cell from that shown in Fig. 8A.

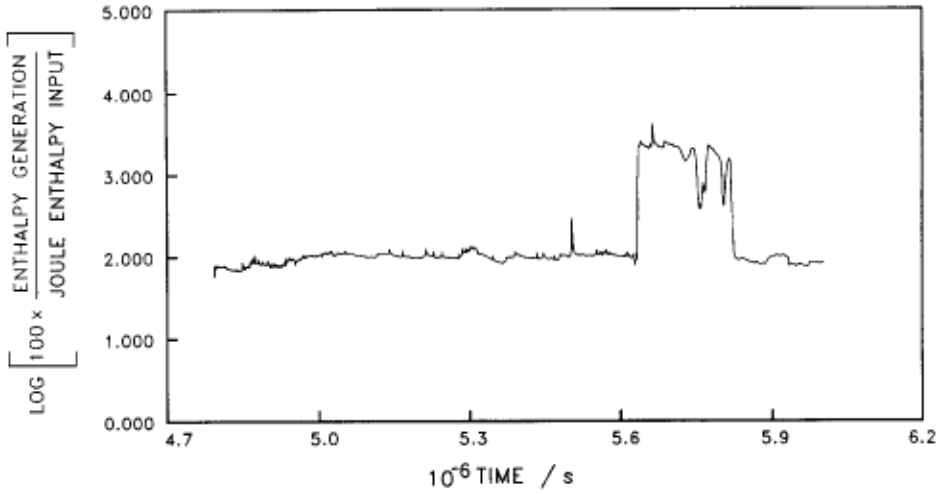

Fig. 9A. Rate of excess enthalpy generation as a function of time for the cell in Fig. 8A.

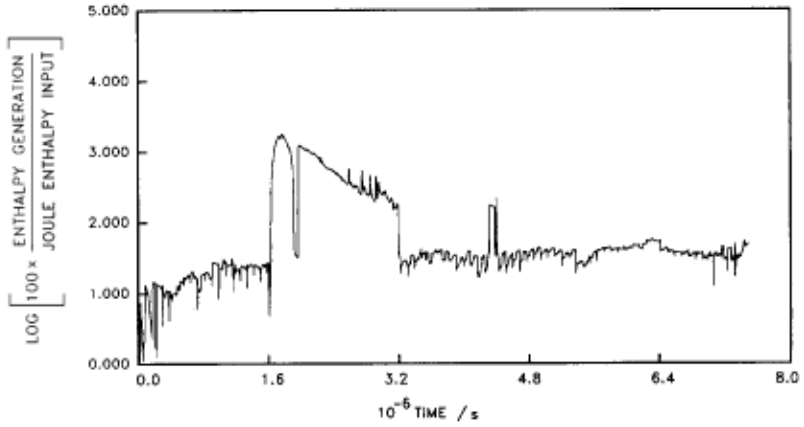

Fig. 9B. Rate of excess enthalpy generation as a function of time for the cell in Fig. 8B.

It is also not possible to decide at this stage whether the attainment of boiling is due to a burst in enthalpy production or to an increase in the baseline output since we have adopted a policy of discontinuing the experiments (or, at least, of reducing the current density) when the boiling point is reached. The reasons for this are as follows: the dissolution of D in Pd is exothermic under these conditions; rapid increases of temperature must therefore be accompanied by a marked increase in the chemical potential (fugacity) of dissolved D^+ since chemical equilibrium cannot be established by the relatively slow diffusional relaxation processes. *We reiterate the warning which we gave in the preliminary publication: such conditions should be avoided at the present stage of research since they could lead to uncontrollable energy releases.* We also draw attention to the fact that rapid increases of temperature are accompanied by marked increases in the rate of generation of tritium. Other aspects of the phenomenon of bursts are covered in the Discussion.

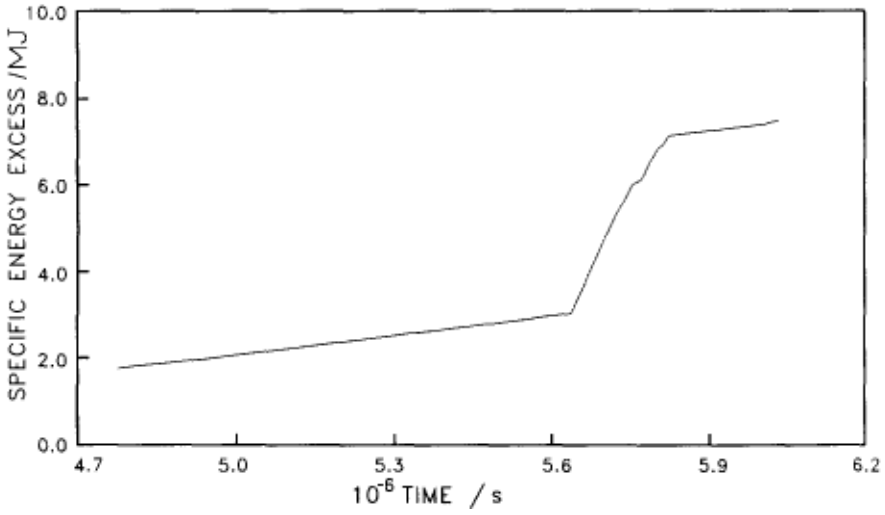

Fig. 10A. Total specific excess energy output as a function of time for the cell in Fig. 8A.

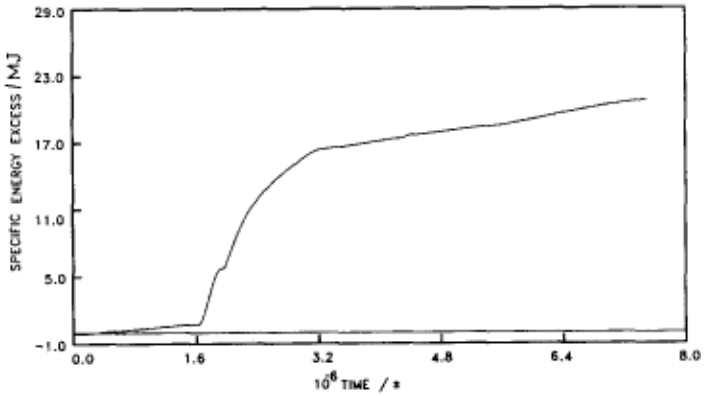

Fig. 10B. Total specific excess energy output as a function of time for the cell in Fig. 8B.

DISCUSSION

The results for the excess enthalpy generation, Table 3, show that very accurate values of the heat flows can be obtained by means of the simple calorimetric technique adopted and this applies equally to the other parameters of the "black box" model. The reason for this high accuracy is the very large redundancy of the data set which consists of ~ 1000 measurements of a highly structured $\vartheta - t$ profile which is used to determine the four parameters of the "black box" model (the fifth parameter is determined from the E_{cell}-t profile). This statement about the accuracy applies to the random errors but we emphasize again that the method of calculation leads to a systematic underestimation which can, however, readily be corrected for using Table A2.1 to give results correct to better than 1%. Statements which have been made about the accuracy of this particular technique [13-15] can be seen to be quite incorrect.

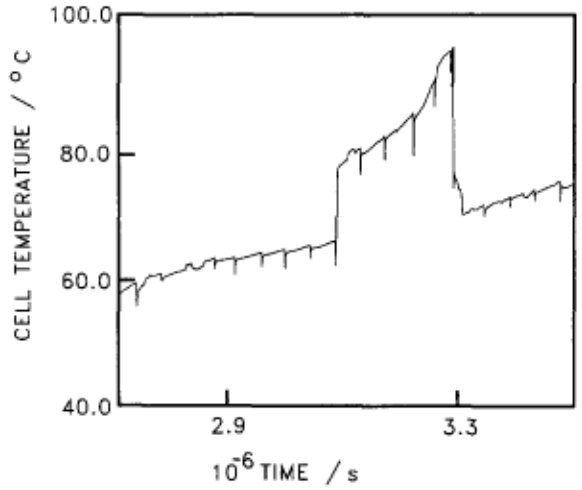

Fig. 11. Cell temperature vs. time plot for a 0.4 × 1.25 cm Pd electrode in 0.1 M LiOD for a period during which the cell went to boiling.

The above statements about the accuracy are borne out by the blank experiments. Table 4 shows that the calorimetric technique adopted gives satisfactory thermal balances for electrolysis according to reaction (i) or for

$$2\ H_2O \rightarrow 2\ H_2 + O_2 \qquad \text{(iv)}$$

for a wide range of conditions and systems. We regard the experiments on the 0.8 cm diameter Pd electrodes in D_2O as the most significant blanks and point out that a blank experiment of this kind was in fact included in our preliminary note (sheet electrode at 0.8 mA cm^{-2}). In common with numerous other investigations we have therefore also carried out experiments on the Pd/D system which give zero excess enthalpy! * The marked excess enthalpy generation for experiments such as those listed in Table 3 must be viewed in the light of these blank experiments. The specific excess enthalpy generation can reach rates as high as 100 W cm^{-3}; this is a factor ~ 5 higher than the highest value which we reported previously [1] and is comparable to the highest value achieved in a recent investigation using Seebeck calorimetry [12]. The values of the excess enthalpy listed in Table 3 are also broadly in line with the results contained in a number of other reports (e.g. see ref. 11) for comparable experimental conditions.

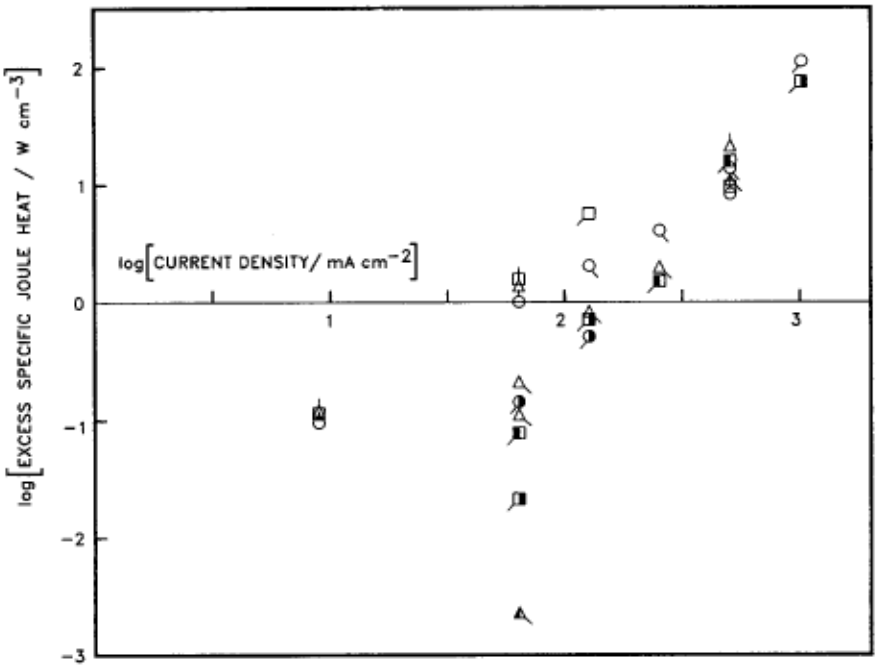

Fig. 12. Log-log plot (excess enthalpy vs. cuffent density) of the data in Tables 3 and A6.1.

It should be noted that the present data support the view that the "steady-state" enthalpy generation is due to a process or processes in the bulk of the electrodes although this statement does not now seem to be as clear cut as that made on the basis of the results contained in the preliminary publication [1]. The data presented here show in more detail that the rates of excess enthalpy production increase markedly with current density, Fig. 12 (the rate of increase is at least on the order I^2), so much so that the process has the appearance of a threshold phenomenon. Experiments of higher precision at low current densities are needed, however, to decide whether this is the case, and if so, what the threshold current density or potential might be. At the highest current densities there is no discernible systematic difference between the data for the different batches of electrodes and electrolytes used in these experiments. The scatter in the results is relatively small at these high current densities but this scatter becomes very large at low to intermediate current density. This variability is much larger than the errors of the individual

* Excess enthalpy generation on 0.8 cm diameter electrodes has been only recently achieved by us using a new batch of electrode material.

measurements of Q_f (Table 3). The scatter must therefore reflect the variability in the experimental conditions such as differences in the electrode materials and/or solution conditions but it could also be that the fugacity of the deuterons in the lattice is more sensitive to the nature of the surface for measurements at low to intermediate current densities. The absence of excess enthalpy generation for 0.8 cm diameter electrodes drawn from Batch 1 certainly points to the importance of the metallurgical history of the specimens in determining Q_f. We note that most investigations reported to date have used relatively low current densities and this may well account for some of the variability of the results. Furthermore the calorimetric techniques and methods of data evaluation adopted in many of these investigations would not allow the accurate measurement of low values of the excess enthalpy. We also note that it is incorrect to derive the error limits from the standard deviation of measurements of Q_f (as has been done in most investigations); these error limits must be derived for each individual measurement of Q_f as has been described above.

Statements as to the magnitudes of the total excess enthalpy are clearly arbitrary since these depend on the duration of any particular experiment: measurements giving excesses of ~ 50 MJ cm^{-3} have now been carried out. The total specific excess enthalpies in the enthalpy bursts are perhaps better defined quantities in this regard. Figures 10A and 10B give the data for the largest bursts we have observed to date and it is of interest that these total enthalpies in the bursts are also far above the values which can be attributed to any chemical reactions. Furthermore, for these bursts, the rates of enthalpy production are up to 17 times (plateau levels) and 40 times (peak values) the total enthalpy inputs to the cells. We note that the use of energy efficient systems (D_2 ionization at the anode, small interelectrode gaps, high electrolyte concentrations) would give energy producing systems even for some of the base line excess enthalpies already reported. During "bursts" the system we have described is an effective energy producer even in its present inefficient form (oxygen evolution at the anode, relatively large anode-cathode spacing, low conductivity electrolyte). As we have pointed out previously [1] the use of energy efficient systems would allow the construction of effective heat generation systems even if the excess enthalpy generation were restricted to the baseline values of Table 3.

It is not possible to decide at this time whether the production of the baseline excess enthalpy and that of the bursts in enthalpy are related processes, and if so, how these phenomena might be linked. Furthermore, it is not clear whether the production of tritium is linked in any causal way to the production of enthalpy although tritium levels in the electrolyte certainly increase markedly following the bursts in enthalpy (increases of up to eight times background have been observed [24]). It may well be, therefore, that we need to consider three separate processes (or six if both bulk and surface reactions are involved).

The contents of this report have been restricted to the calorimetric results and other data will be discussed elsewhere [19]. Nevertheless we close this paper with some further comments and speculations. The preliminary note was to have been published under the title "Electrochemically Induced Fusion of Deuterium?" but the all important question mark was omitted. It is our view that there can be little doubt that one must invoke nuclear processes to account for the magnitudes of the enthalpy releases, although the nature of these processes is an open question at this stage. [*] It should be apparent to unbiased readers that, contrary to what has been stated

[*] It is hardly tenable that the substantial number of confirmations of the calorimetric data using a variety of techniques can be explained by a collection of different systematic errors nor that tritium generation can be accounted for by any but nuclear processes.

frequently, we did not in fact make any specific suggestions on this score in our first publication [1]. Certainly, we suggested that these processes must be due to highly compressed deuterons and that these might be located at multiply occupied octahedral sites in the lattice. Palladium has a relatively low cohesive strength so that these sites will distort to allow such multiple occupancy at high deuteron activities although such sites might then be more accurately described as being part of dislocation loops. Grain boundaries and larger scale voids are further possible special sites. It should be noted that electrodes used under the conditions employed here become highly dislocated. Clusters of deuterons would be in effect nuclei of metallic deuterium and the boson character of the particles would play a special role in determining the outcome of collisions in these clusters. That the boson character of the deuterons is important in motion throughout the lattice is shown clearly by comparisons of the diffusion coefficients of H, D, and T in palladium (e.g. see ref. 25). Parts of the clusters could function as spectators in any nuclear reactions although other types of negatively charged and especially neutral spectators could also be involved. [**]

We note finally that the deuterons in the lattice are similar to low ion temperature plasmas (~ 1 eV) and that fusion of low energy deuterons was already observed [27,28] in $(ND_4)_2SO_4$ targets at the time of the discovery of the major nuclear reaction paths of deuterium [4] (called diplogen at that time). It appears that this fact has been forgotten by the scientific community as has been the evident induction of fusion in high density, low ion temperature quiescent deuterium gas plasmas generated and maintained in magnetic mirror devices by means of electron cyclotron resonance [29]. Deuterons in the Pd host lattice clearly can be regarded as an example of very high density low ion temperature plasmas; the fate of the nuclear reaction(s) in this case is evidently markedly modified by the presence of the host lattice.

ACKNOWLEDGEMENTS

The authors thank the Office of Naval Research and the University of Utah for financial support of various phases of this work. We thank Johnson-Matthey PLC for the loan of all of the metal electrodes used in this work. Finally, we appreciate the forbearance of our families and friends during our period of tribulation which is now thankfully approaching its end.

[**] At a recent meeting on Solid State Fusion [26], Edward Teller proposed that a neutral Schlepton takes part in such nuclear processes. Our own discussions on this point led us to name such a particle as Meschuggenon, a name more in keeping with the nature of this field of research.

APPENDIX 1

Some general considerations about the calorimetry of electrode processes

It is evident that in calorimetric measurements on working electrochemical systems the enthalpy is generated at the electrode surfaces with the exception of that part due to Joule heating of the electrolyte. This heat generation is coupled to heat removal through one or more heat transfer surfaces. It is therefore necessary to design the calorimeters in such a way as to reduce as far as possible the effects of this non-uniform injection and removal of heat. A number of steps which can be taken are elementary. Thus, for example, the design of Fig. 1 ensures the axially uniform injection of heat throughout the calorimeter.

For the particular case under consideration, where vigorous gas evolution takes place at both electrodes, the transport of heat from the electrode surfaces and equalization of temperature differences will be dominated by convective mixing by eddies induced in the boundary layers and their decay by eddy diffusion into the bulk of the liquid. The use of long narrow calorimeters ensures rapid radial mixing; the slower axial mixing (see the main text) is then of small importance in view of the axially uniform injection and removal of heat.

The eddies in the system will evidently have a range of length scales, but here we will consider that they can be characterized by a single mean length, l (in cm) (a more comprehensive discussion of the behaviour of such calorimeters will be given elsewhere [19]). This length will naturally decrease markedly with increasing rates of stirring. The order of magnitude of the number of eddies for a system which contains as much surface as the calorimeter in Fig. 1 will be ~ V/l^3 where V (in cm^3) is the electrolyte volume. Since the generation of eddies takes place at random, the standard deviation of this number will be ~ $(V/l^3)^{1/2}$ and the order of magnitude of the fluctuating eddy volume will be ~ $(Vl^3)^{1/2}$. We will assume here that there will be a characteristic temperature difference, $\delta\vartheta$ (in K) between the eddies when these are generated and the bulk of the liquid. Then the variance of the enthalpy of the calorimeter will be $\left[\left(C_{P,D_2O,l}/m_{D_2O}\right)\rho_{D_2O}\left(Vl^3\right)^{1/2}\delta\vartheta\right]^2$ where m_{D_2O} (g mol^{-1}) is the molecular weight of D_2O and ρ_{D_2O} (in g cm^{-3}) is the density and this variance will set a limit on the accuracy of the calorimeter. At a more exact level, we would expect that the fluctuating enthalpy content, W (in J) will be characterized by an autocorrelation function

$$\Phi(W) \cong \left[\frac{C_{P,\mathrm{D_2O},l}}{m_{\mathrm{D_2O}}}\rho_{\mathrm{D_2O}}(Vl^3)^{1/2}\delta\vartheta\right]^2 \exp\left(\frac{-D_{\mathrm{eddy}}t}{r^2}\right) \qquad \text{(A1.1)}$$

where D_{eddy} (in $cm^2\ s^{-1}$) is an eddy diffusivity and r (in cm) is the shortest length scale over which eddies decay; the order of magnitude of this scale for the calorimeter design in Fig. 1 will be its radius. Fluctuations in the enthalpy content will be characterized by the power spectral density

$$G(W) \cong \mathrm{Re}\left[\frac{C_{P,\mathrm{D_2O},l}}{m_{\mathrm{D_2O}}}\rho_{\mathrm{D_2O}}(Vl^3)^{1/2}\delta\vartheta\right]^2\int_0^\infty \exp\left[-\left(\frac{D_{\mathrm{eddy}}}{r^2}+\mathrm{j}\omega\right)\right]t\,\mathrm{d}t$$

$$= \mathrm{Re}\left[\frac{C_{P,\mathrm{D_2O},l}}{m_{\mathrm{D_2O}}}\rho_{\mathrm{D_2O}}(Vl^3)^{1/2}\delta\vartheta\right]^2\left(\frac{\tau}{1+\mathrm{j}\omega\tau}\right)$$

$$= \left[\frac{C_{P,\mathrm{D_2O},l}}{m_{\mathrm{D_2O}}}\rho_{\mathrm{D_2O}}(Vl^3)^{1/2}\delta\vartheta\right]^2\left(\frac{\tau}{1+\omega^2\tau^2}\right) \qquad \text{(A1.2)}$$

where

$$\tau = \left(r^2/D_{\mathrm{eddy}}\right) \qquad \text{(A1.3)}$$

is the relaxation time for eddy diffusion. At a more exact level, we should evaluate the spatial averages of the appropriate cross-correlation functions and determine the relevant cross-power spectral densities.

On the long time scales at which calorimetric measurements are made, the power spectral density eqn. (A1.2) becomes white

$$G(W) \cong \left[\frac{C_{P,\mathrm{D_2O},l}}{m_{\mathrm{D_2O}}}\rho_{\mathrm{D_2O}}(Vl^3)^{1/2}\delta\vartheta\right]^2\tau = \left[\frac{C_{P,\mathrm{D_2O},l}}{m_{\mathrm{D_2O}}}\rho_{\mathrm{D_2O}}(Vl^3)^{1/2}\delta\vartheta\right]^2\left(\frac{r^2}{D_{\mathrm{eddy}}}\right) \qquad \text{(A1.4)}$$

and this sets a limit on the accuracy with which measurements can be made using any particular calorimeter.

We can draw a number of conclusions from eqn. (A1.4) about the design criteria of suitable calorimeters: it is favorable to use systems of small volume and intense stirring which reduces $G(W)_{\omega\to 0}$ by virtue of increasing D_{eddy} and decreasing V and l; it is also favorable to insure that mixing takes place over a short distance at least with regard to one dimension of the calorimeter and the use of designs having one short dimension also ensures that l is small; finally, we would expect $\delta\vartheta$ to increase with the rates of heat transfer across the electrode and cell wall surfaces and it is therefore favorable to reduce these as far as possible and to scale the system so that nevertheless adequately large values of $\Delta\vartheta$ are established.

The implications and generality of these restrictions have sometimes not been appreciated; the multiple effects of increases in the electrolyte volume on the increase of l and r and a decrease in D_{eddy} are especially serious in this regard. Naturally, there are other factors which will degrade the performance further. Randomly fluctuating signals, which must contribute to the power spectral density at low frequencies, (such as fluctuations in the heat transfer rates induced by flow calorimetry and sources of 1/f noise) are particularly serious in degrading the performance.

With these criteria in mind, we have designed long, thin, cylindrical calorimeters for this work. We emphasize that we have found it essential to evolve the calorimeter design by a stepwise

iterative process as it is necessary to scale the calorimeter and the electrodes so that the excess enthalpies become large compared to the experimental errors.

APPENDIX 2

The definition, determination, and application of the heat transfer coefficients governing the behavior of electrochemical Dewar type calorimeter cells

The exact expression for the rate of heat transfer Q (in W) in a Dewar-type open cell is governed by a mixture of radiation and conduction. For steady state heat release Q_1 (in W) at a cell temperature $\vartheta_{cell,1}$ (K) we have:

$$\begin{aligned} Q_1 &= k_R\left[\vartheta_{cell,1}^4 - \vartheta_{bath}^4\right] + k_C\left[\vartheta_{cell,1} - \vartheta_{bath}\right] \\ &= k_R\left[(\vartheta_{bath} + \Delta\vartheta_1)^4 - \vartheta_{bath}^4\right] + k_C\,\Delta\vartheta_1 \end{aligned} \qquad (A2.1)$$

where k_R (in W K^{-4}) is the heat transfer coefficient due to radiation, k_c (in W K^{-1}) is the heat transfer coefficient due to conduction, and $\Delta\vartheta_1$ (in K) is the difference in temperature between the cell and bath.

We now consider a second set of conditions where the steady state heat release is Q_2 and the cell temperature is $\vartheta_{bath} + \Delta\vartheta_2$. For these conditions, the effect of applying a resistive heating term ΔQ_2 is to raise the cell temperature in the final steady state by $\Delta\Delta\vartheta_2$. For these steady states we have

$$Q_2 = k_R\left[(\vartheta_{bath} + \Delta\vartheta_2)^4 - \vartheta_{bath}^4\right] + k_C\,\Delta\vartheta_2 \qquad (A2.2)$$

and

$$Q_2 + \Delta Q_2 = k_R\left[(\vartheta_{bath} + \Delta\vartheta_2 + \Delta\Delta\vartheta_2)^4 - \vartheta_{bath}^4\right] + k_C\left[\Delta\vartheta_2 + \Delta\Delta\vartheta_2\right] \qquad (A2.3)$$

We consider such a second set of conditions as the heat transfer coefficients may not be evaluated under the same operating conditions as those which pertain to the measurement of heat outputs from the cell (however, see below for further comments on the operating conditions used in this investigation). Subtracting eqn. (A2.2) from eqn. (A2.3) we obtain

$$\Delta Q_2 = k_R\left[(\vartheta_{bath} + \Delta\vartheta_2 + \Delta\Delta\vartheta_2)^4 - (\vartheta_{bath} + \Delta\vartheta_2)^4\right] + k_C\,\Delta\Delta\vartheta_2 \qquad (A2.4)$$

It is convenient to express the conductive heat transfer coefficient in terms of the radiative coefficient

$$k_C = 4\Phi k_R \vartheta_{bath}^3 \qquad (A2.5)$$

so that eqn. (A2.4) becomes

$$\Delta Q_2 = k_R\left\{\left[(\vartheta_{bath} + \Delta\vartheta_2 + \Delta\Delta\vartheta_2)^4 - (\vartheta_{bath} + \Delta\vartheta_2)^4\right] + 4\Phi\vartheta_{bath}^3\,\Delta\Delta\vartheta_2\right\} \qquad (A2.6)$$

We derive the radiative heat transfer coefficient from eqn. (A2.6)

$$k_R = \frac{\Delta Q_2}{\left[(\vartheta_{bath} + \Delta\vartheta_2 + \Delta\Delta\vartheta_2)^4 - (\vartheta_{bath} + \Delta\vartheta_2)^4\right] + 4\Phi\vartheta^3_{bath}\,\Delta\Delta\vartheta_2} \qquad \text{(A2.7)}$$

If we use this heat transfer coefficient to define the rate of heat transfer at the cell temperature $(\vartheta_{bath} + \Delta\vartheta_1)$ we obtain from eqn. (A2.1) with eqn. (A2.5)

$$Q_1 = \frac{\Delta Q_2\left\{\left[(\vartheta_{bath} + \Delta\vartheta_1)^4 - \vartheta^4_{bath}\right] + 4\Phi\vartheta^3_{bath}\,\Delta\vartheta_1\right\}}{\left[(\vartheta_{bath} + \Delta\vartheta_2 + \Delta\Delta\vartheta_2)^4 - (\vartheta_{bath} + \Delta\vartheta_2)^4\right] + 4\Phi\vartheta^3_{bath}\,\Delta\Delta\vartheta_2} \qquad \text{(A2.8)}$$

Equation (A2.8) therefore allows for the fact that the measurement of the heat output Q_1 is not necessarily made at the same temperature as that at which the heat transfer coefficient is determined.

The application of eqn. (A2.8) requires the determination of Φ, i.e. in effect, the separate determination of k_R and k_C. While methods can be devised for this separation into the radiative and conductive terms, these methods always appear to depend in effect on the differentiation of the experimental measurements with respect to $\Delta\vartheta$. Such procedures therefore invariably reduce the accuracy of the data evaluation. Since the conductive contribution to the heat transfer will always be smaller than the radiative term, a sounder approach is to investigate the error introduced by ignoring the conductive contribution. We compensate for this neglect of the conductive term by making an appropriate increase in the radiative heat transfer coefficient.

$$k'_R = \frac{\Delta Q_2}{\left[(\vartheta_{bath} + \Delta\vartheta_2 + \Delta\Delta\vartheta_2)^4 - (\vartheta_{bath} + \Delta\vartheta_2)^4\right]} \qquad \text{(A2.9)}$$

which now becomes an effective heat transfer coefficient. We use eqn. (A2.9) to calculate the approximate value of the heat transfer rate

$$Q'_1 = \frac{\Delta Q_2\left[(\vartheta_{bath} + \Delta\vartheta_1)^4 - \vartheta^4_{bath}\right]}{\left[(\vartheta_{bath} + \Delta\vartheta_2 + \Delta\Delta\vartheta_2)^4 - (\vartheta_{bath} + \Delta\vartheta_2)^4\right]} \qquad \text{(A2.10)}$$

In this approximate value of the heat output from the cell we therefore allow for the neglect of the conductive heat transfer term by making an appropriate increase in the radiative term. We can test the validity of this approximation by examining how far the ratio Q'_1/Q_1 deviates from unity. We have

$$\frac{Q'_1}{Q_1} = \frac{\left[(\vartheta_{bath} + \Delta\vartheta_1)^4 - \vartheta^4_{bath}\right]}{\left[(\vartheta_{bath} + \Delta\vartheta_2 + \Delta\Delta\vartheta_2)^4 - (\vartheta_{bath} + \Delta\vartheta_2)^4\right]} \times \frac{\left[(\vartheta_{bath} + \Delta\vartheta_2 + \Delta\Delta\vartheta_2)^4 - (\vartheta_{bath} + \Delta\vartheta_2)^4\right] + 4\Phi\vartheta^3_{bath}\,\Delta\Delta\vartheta_2}{\left[(\vartheta_{bath} + \Delta\vartheta_1)^4 - \vartheta^4_{bath}\right] + 4\Phi\vartheta^3_{bath}\,\Delta\vartheta_1} \qquad \text{(A2.11)}$$

For the special case of the determination of k'_R at the same operating conditions as those for the measurement of Q_1 (which is, in fact, the procedure which has been used throughout this work), we can drop the subscripts 1 and 2 and write

$$\frac{Q'_1}{Q_1} = \frac{\left[(\vartheta_{\text{bath}} + \Delta\vartheta)^4 - \vartheta_{\text{bath}}^4\right]}{\left[(\vartheta_{\text{bath}} + \Delta\vartheta + \Delta\Delta\vartheta)^4 - (\vartheta_{\text{bath}} + \Delta\vartheta)^4\right]}$$

$$\times \frac{\left[(\vartheta_{\text{bath}} + \Delta\vartheta + \Delta\Delta\vartheta)^4 - (\vartheta_{\text{bath}} + \Delta\vartheta)^4\right] + 4\Phi\vartheta_{\text{bath}}^3\,\Delta\Delta\vartheta}{\left[(\vartheta_{\text{bath}} + \Delta\vartheta)^4 - \vartheta_{\text{bath}}^4\right] + 4\Phi\vartheta_{\text{bath}}^3\,\Delta\vartheta} \qquad \text{(A2.12)}$$

The ratios Q'_1/Q_1 defined in eqns. (A2.11) and (A2.12) therefore give estimates of the effects of the neglect of the conductive heat transfer term (with a compensating increase of the radiative term) on the measurement of the heat output from the cells.

Table A2.1 shows the variation of Q'_1/Q_1 with $\Delta\vartheta$ for $\Phi = 0.05$ to 1.0 and using the likely value of $\Delta\Delta\vartheta = 2$ K. The probable domain of measurement is delineated by the dotted lines. It can be seen that the errors introduced by neglecting the conductive term and by allowing for this by making an appropriate increase in k_R are less than 4%. Correction of the heat transfer using the known values of Φ (see the main text) allows the estimation of the heat output to better than 1%. It should be noted that this assumption leads to an *underestimate* of the heat output from the cell. Furthermore, for measurements under more extreme conditions, the underestimates are larger.

The variation of Q'_1/Q_1 with $\Delta\vartheta_1$ for various values of $\Delta\vartheta_2$ and for the single value $\Phi = 0.50$ and again using $\Delta\Delta\vartheta = 2$ K is shown in Table A2.2. We observe that there are again only small deviations from unity and that these are negative provided the calibrations are carried out at a temperature above that at which the heat transfer rate is determined. We obtain only small positive deviations of Q'_1 from Q_1 if the calibrations are made at low temperatures while the heat transfer rate is determined at very high temperatures. We have avoided such conditions throughout this work.

TABLE A2.2

Variation of Q'/Q with $\Delta\vartheta_1$ and $\Delta\vartheta_2$ for $\Phi = 0.50$

$\Delta\vartheta_1/K$	$\Delta\vartheta_2/K$							
	5	10	15	. 20	25	30	35	40
5	0.989	0.974	0.960	. 0.947	0.935	0.923	0.912	0.902
10	0.997	0.982	0.968	. 0.955	0.942	0.930	0.919	0.909
15	1.005	0.990	0.975	. 0.962	0.950	0.938	0.927	0.916
. . . . .								
20	1.013	0.997	0.983	0.970	0.957	0.945	0.934	0.923
25	1.020	1.005	0.990	0.977	0.964	0.952	0.941	0.930
30	1.028	1.012	0.998	0.984	0.971	0.959	0.948	0.937
35	1.035	1.020	1.005	0.991	0.978	0.966	0.955	0.944
40	1.043	1.027	1.012	0.998	0.985	0.973	0.962	0.951

Linearization of the equations

In the derivation of closed form solutions for the behavior of Dewar cell calorimeters and for the evaluation of approximate values of the heat transfer coefficients and of the heat outputs it is convenient to use the linearized form of eqn. (A2.1)

$$Q_1 \cong 4k_R \vartheta_{bath}^3 \, \Delta\vartheta_1 + k_C \, \Delta\vartheta_1 = 4k_R \vartheta_{bath}^3 (1 + \Phi) \, \Delta\vartheta_1 = 4k_R'' \vartheta_{bath}^3 \, \Delta\vartheta_1 \qquad \text{(A2.13)}$$

where k_R'' (in W K$_{-4}$) is an effective heat transfer coefficient which applies to such linearized equations. Application of the same calibration procedure as that leading to eqn. (A2.4) gives

$$\Delta Q_2 \cong 4k_R''(\vartheta_{bath} + \Delta\vartheta_2)^3 \, \Delta\Delta\vartheta_2 = 4k_R'' \vartheta_{cell}^3 \, \Delta\Delta\vartheta_2 \qquad \text{(A2.14)}$$

Such linearizations can apply only for values of the cell temperature close to that of the bath temperature (say 2 K < $\Delta\Delta\vartheta$ < 5 K) [15,22]. We have used the linearization (A2.13) in order to obtain a closed form solution for the behavior of the calorimeter (see Appendix 4).

Effect of the temperature drops across the cell walls on the integral heat transfer coefficient and heat transfer

As the radiative heat transfer takes place between the faces on the vacuum sides of the Dewar vessels, the radiative heat transfer is inevitably in series with conductive terms governing heat transfer through the walls. It is therefore necessary to assess the effects of these temperature drops across the cell walls on the evaluation of the heat transfer from the cell to the surrounding water bath. For the sake of simplicity, we will assume that there are identical temperature drops $\delta\vartheta_2$ across both the inner and outer walls of the Dewars and we ignore any other parallel conductance path i.e. we formulate the problem immediately in terms of an effective radiative heat transfer coefficient. Furthermore we carry out a linearization as in eqn. (A2.13). We obtain

$$\begin{aligned} Q_2 = k_C \delta\vartheta_2 &= k_R''' \left[(\vartheta_{bath} + \Delta\vartheta_2 - \delta\vartheta_2)^4 - (\vartheta_{bath} + \delta\vartheta_2)^4 \right. \\ &\cong k_R''' \left[4\vartheta_{bath}^3 \, \Delta\vartheta_2 - 8\vartheta_{bath}^3 \delta\vartheta_2 \right] \end{aligned} \qquad \text{(A2.15)}$$

where k_R'' (in W K^{-4}) is the relevant effective radiative heat transfer coefficient. Similarly for the steady state attained when applying the resistive joule heating input ΔQ_2,

$$\begin{aligned} Q_2 + \Delta Q_2 &= k_C (\delta\vartheta_2 + \delta\delta\vartheta_2) \\ &= k_R''' \left[(\vartheta_{bath} + \Delta\vartheta_2 + \Delta\Delta\vartheta_2 - \delta\vartheta_2 - \delta\delta\vartheta_2)^4 - (\vartheta_{bath} + \delta\vartheta_2 + \delta\delta\vartheta_2)^4 \right] \\ &\cong k_R''' \left[4\vartheta_{bath}^3 (\Delta\vartheta_2 + \Delta\Delta\vartheta_2) - 8\vartheta_{bath}^3 (\delta\vartheta_2 + \delta\delta\vartheta_2) \right] \end{aligned} \qquad \text{(A2.16)}$$

where $\delta\delta\vartheta_2$ is the additional temperature drop across the glass walls due to the input ΔQ_2. From eqns. (A1.15) and (A1.16)

$$\Delta Q_2 = k_R''' \left[4\vartheta_{bath}^3 \, \Delta\Delta\vartheta_2 - 8\vartheta_{bath}^3 \delta\delta\vartheta_2\right] \tag{A2.17}$$

and

$$k_R''' = \frac{\Delta Q_2}{4\vartheta_{bath}^3 \, \Delta\Delta\vartheta_2 - \delta\vartheta_{bath}^3 \delta\delta\vartheta_2} \tag{A2.18}$$

Within the limits of the approximation, we then obtain an expression for the heat flow

$$\begin{aligned} Q_1''' &= k_R''' \left[(\vartheta_{bath} + \Delta\vartheta_1 - \delta\vartheta_1)^4 - (\vartheta_{bath} + \delta\vartheta_1)^4\right] \\ &\cong k_R''' \left[4\vartheta_{bath}^3 \, \Delta\vartheta_1 - 8\vartheta_{bath}^3 \delta\vartheta_1\right] = \Delta Q_2 \frac{(\Delta\vartheta_1 - 2\delta\vartheta_1)}{(\Delta\Delta\vartheta_2 - 2\delta\delta\vartheta_2)} \end{aligned} \tag{A2.19}$$

If we neglect the temperature drops $\delta\vartheta_1$ and $\delta\vartheta_2 + \delta\delta\vartheta_2$ across the cell walls, we obtain an approximate value of the heat flux, Q_1'', appropriate to the linearized form of the equations

$$Q_1'' = \Delta Q_2 \frac{\Delta\vartheta_1}{\Delta\Delta\vartheta_2} \tag{A2.20}$$

We can assess the deviation of Q_1'' from Q_1''' by taking the ratio

$$\begin{aligned} \frac{Q_1''}{Q_1'''} &= \frac{\Delta\vartheta_1}{\Delta\Delta\vartheta_2} \frac{(\Delta\Delta\vartheta_2 - 2\delta\delta\vartheta_2)}{(\Delta\vartheta_1 - 2\delta\vartheta_1)} = \left(1 - \frac{2\delta\delta\vartheta_2}{\Delta\Delta\vartheta_2}\right)\left(1 - \frac{2\delta\vartheta_1}{\Delta\vartheta_1}\right)^{-1} \\ &\cong 1 - \frac{2\delta\delta\vartheta_2}{\Delta\Delta\vartheta_2} + \frac{2\delta\vartheta_1}{\Delta\vartheta_1} = 0 \end{aligned} \tag{A2.21}$$

since the temperature drops across the cell walls will be proportional to A4. It follows that the definition of the heat transfer coefficient which neglects the effects of conductivity through the cell walls allows an estimation of the heat output which automatically corrects for the neglect of these temperature changes. Furthermore, any other linear perturbation of the integral heat transfer coefficient is automatically allowed for when estimating the heat output of the cell provided the heat transfer coefficient is determined from the resistive joule heating input calibration. It should be noted also that evaluations of the heat output based on eqn. (A2.10) optimize the accuracy (apart from the *systematic* underestimate of this heat output) since we avoid any splitting of the heat transfer coefficient into the radiative and conductive terms and since the individual absolute temperatures are known to high precision.

APPENDIX 3

"Black box" models of the calorimeter

In common with all other physicochenical and engineering devices, the evaluation of data from the behavior of the Dewar-type electrochemical calorimeters requires the construction of accurate "black box" models, Fig. A3.1. In this particular case, the models must account for the enthalpy and mass balances in the cell; these can be combined conveniently through the current efficiency, y, of the electrolysis.

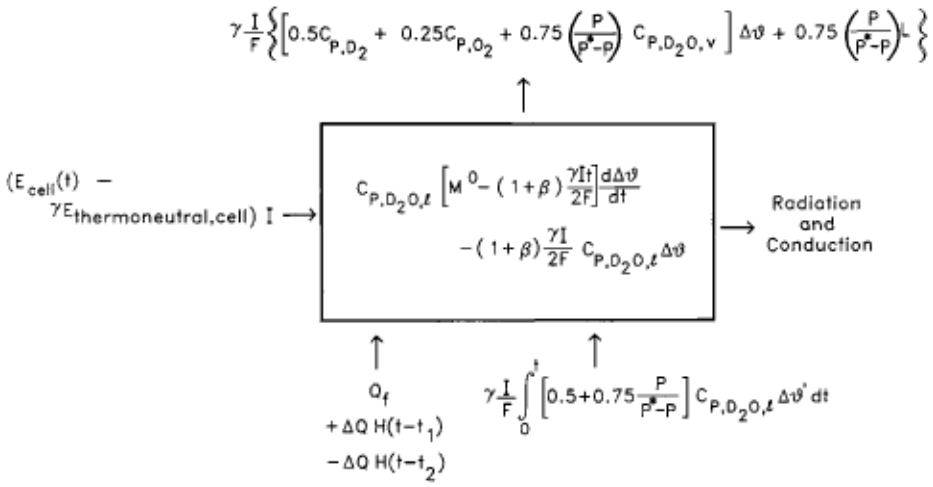

Fig. A3.1. Complete "black box" representation of the heat flows in the Dewar calorimeters used in this work.

The nature of most of the enthalpy flows into and out of the "black box" is readily apparent. Thus:

(a) The enthalpy input to the cell

$$\left(E_{\text{cell}}(t) - E_{\text{thermoneutral,cell}}\gamma\right)I = \left[-\frac{\Delta G^{\ominus}}{2F} + \eta_{\text{anodic}}(t) - \eta_{\text{cathodic}}(t) + \eta_{\text{ohmic}}(t) + \frac{\gamma\,\Delta H^{\ominus}}{2F}\right]I \qquad \text{(A3.1)}$$

Here $E_{\text{cell}}(t)$ is the measured cell voltage which is the sum of the reversible potential and all irreversible work terms $(\eta_{\text{anodic}}(t)\text{-}\eta_{\text{cathodic}}(t)+\eta_{\text{ohmic}}(t))I$ and where the anodic and cathodic overpontentials are taken to include both the activation and concentration terms. This detailed decomposition of E_{cell} is of no further interest since all such irreversibilities are automatically included in the experimental measurements. The term Ehermoneutralcell is the cell voltage at which the electrolysis is thermoneutral; this differs from the reversible potential of the reaction

$$D_2 + \tfrac{1}{2}\,O_2 \rightleftharpoons D_2O \qquad \text{(i)}$$

since the electrolysis proceeds with an increase of entropy.

The thermodynamic quantities in eqn. (A3.1) have been written for the values in the standard states at the cell temperature; the effects of changes in activity of the electrolyte on ΔG can be included in the overpotential terms and are of no further interest since E_{cell} is a measured quantity; the effects of changes in activity of the D_2O on ΔH due to the addition of electrolyte are second order small quantities.

(b) The enthalpy of the gas stream

The term

$$\frac{\gamma I}{F}\left\{\left[0.5C_{P,\mathrm{D_2}} + 0.25C_{P,\mathrm{O_2}} + 0.75\left(\frac{P}{P^* - P}\right)C_{P,\mathrm{D_2O,v}}\right]\Delta\vartheta + 0.75\left(\frac{P}{P^* - P}\right)\mathrm{L}\right\} \tag{A3.2}$$

is the enthalpy content of the gas stream relative to the enthalpy content at the temperature of the thermostat. The heat capacitances have been taken to be independent of the temperature and the gas stream has been assumed to be saturated with D_2O vapor at the partial pressure P which applies to the cell temperature; P^* is the atmospheric pressure and L is the enthalpy of evaporation of D_2O which has been assumed to be independent of temperature.

(c) The heat transfer from the cell

The integral heat transfer term can be written in a variety of ways depending on the properties of the calorimeter and the chosen level of approximation, e.g. the forms (A2.1), (A2.6), (A2.10), or (A2.13) discussed in Appendix 2. However, for a continuously reacting chemical system (open system) such as that in the electrochemical Dewar cells, the cell contents change with time. In consequence the heat transfer coefficients are time-dependent and this also affects the heavy water equivalent of the cell (see (*f*) below). The extent of radiant surface decreases with time while the length of any parallel conduction path increases with time. At the first level of approximation we would therefore expect the integral heat transfer coefficients to decrease linearly with time. For example, using eqns. (A2.1) and (A2.5) we can write the heat transfer as

$$k_{\mathrm{R}}^{\circ}\vartheta_{\mathrm{bath}}^3\left[1 - \frac{(1+\lambda)\gamma I t}{2FM^{\circ}}\right]\left[\left[\frac{(\vartheta_{\mathrm{bath}} + \Delta\vartheta)^4 - \vartheta_{\mathrm{bath}}^4}{\vartheta_{\mathrm{bath}}^3}\right] + 4\Phi\,\Delta\vartheta\right] \tag{A3.3}$$

where the term λ allows for a more rapid decrease of the radiant surface area (and increase of the length of the conduction path) than would be predicted by electrolysis alone in view of the effects of the internal solid cell components (glass rods, tubes). The superscripts zero here (and elsewhere) denote values at a chosen time origin.

(d) The enthalpy of the make-up stream

The term

$$\frac{\gamma I}{F}\int_0^t\left[0.5 + 0.75\left(\frac{P}{P^* - P}\right)\right]C_{P,\mathrm{D_2O,l}}\,\Delta\vartheta'\,\mathrm{d}t \tag{A3.4}$$

is the enthalpy flow due to the addition of liquid D_2O to make up for the losses due to electrolysis and evaporation. Here $\Delta\vartheta'$ is the difference in temperature between the cell and the make-up stream. It was found that the quantity to be added was given accurately by this expression at low and intermediate temperatures (for $\Delta\vartheta$ < 20 K). In practice, it was found to be convenient to add heavy water at fixed time intervals (see the main text). Provided consideration of the $\vartheta - t$ profile is restricted to times longer than six thermal relaxation times following the addition of D_2O, the effects of this term can be neglected.

(e) The excess enthalpy generation

$Q_f(t)$ is the time dependent excess enthalpy generation and $\Delta QH(t - t_1)$ - $\Delta QH(t - t_2)$ is the enthalpy input from the resistive heater used to calibrate the system; here $H(t - t_1)$ and $H(t - t_2)$ are the Heaviside unity functions and the input ΔQ is confined to the time $t_1 < t < t_2$.

(f) The enthalpy content of the calorimeter

A general expression for the water equivalent is

$$M = M^\circ - (1+\beta)\gamma It/2F \qquad \text{(A3.5)}$$

where the term β allows for a more rapid decrease of the water equivalent with time than would be predicted by electrolysis alone. β includes the contribution due to evaporation, $1.5\left(P/\left(P^*-P\right)\right)$, but the magnitude of this term is small at low and intermediate temperatures. Other contributions to would also be expected to be small in comparison with λ.

The time dependence of the enthalpy of the calorimeter is obtained by general differentiation of $C_{P,D_2O,l}M\Delta\vartheta$:

$$\frac{\mathrm{d}}{\mathrm{d}t}\left(C_{P,\mathrm{D_2O,l}}M\,\Delta\vartheta\right) = C_{P,\mathrm{D_2O,l}}\left[M^\circ - \frac{(1+\beta)\gamma It}{2F}\right]\frac{\mathrm{d}\,\Delta\vartheta}{\mathrm{d}t} - C_{P,\mathrm{D_2O,l}}\frac{(1+\beta)\gamma I\,\Delta\vartheta}{2F} \qquad \text{(A3.6)}$$

The differential equation governing the behavior of the calorimeter is obtained by equating eqn. (A3.6) to the sum of the heat loss and generation terms in the Dewar:

$$\begin{aligned} &C_{P,\mathrm{D_2O,l}}\left[M^\circ - \frac{(1+\beta)\gamma It}{2F}\right]\frac{\mathrm{d}\,\Delta\vartheta}{\mathrm{d}t} - C_{P,\mathrm{D_2O,l}}\frac{(1+\beta)\gamma I\,\Delta\vartheta}{2F} \\ &\quad = \left(E_{\mathrm{cell}}(t) - \gamma E_{\mathrm{thermoneutral,cell}}\right)I + Q_f(t) + \Delta QH(t-t_1) - \Delta QH(t-t_2) \\ &\qquad - \frac{\gamma I}{F}\left\{\left[0.5C_{P,\mathrm{D_2}} + 0.25C_{P,\mathrm{O_2}} + 0.75\left(\frac{P}{P^*-P}\right)C_{P,\mathrm{D_2O,v}}\right]\Delta\vartheta\right. \\ &\qquad \left. + 0.75\left(\frac{P}{P^*-P}\right)L\right\} \\ &\qquad - k_R^\circ\vartheta_{\mathrm{bath}}^3\left[1 - \frac{(1+\lambda)\gamma It}{2FM^\circ}\right]\left[\left[\frac{(\vartheta_{\mathrm{bath}}-\Delta\vartheta)^4 - \vartheta_{\mathrm{bath}}^4}{\vartheta_{\mathrm{bath}}^3}\right] + 4\Phi\,\Delta\vartheta\right] \end{aligned} \qquad \text{(A3.7)}$$

Equation (A3.7) can be simplified in a number of important regards. In the first place we observe that

$$\Delta H^{\ominus}_{\text{cell}} = \Delta H^{\ominus}_{\text{bath}} + \sum_i \nu_i C_{P,i}\, \Delta\vartheta \tag{A3.8}$$

where the summation is taken over the products D_2 and O_2 and reagent $(D_2O)_1$ in the usual way. Secondly, as has been noted in the main text, the current efficiency for D_2 and O_2 generation is close to unity, i.e. $\gamma = 1$. With these simplification we obtain

$$\begin{aligned} & C_{P,\mathrm{D_2O,l}}\left[M^\circ - \frac{(1+\beta)It}{2F}\right]\frac{\mathrm{d}\,\Delta\vartheta}{\mathrm{d}t} - C_{P,\mathrm{D_2O,l}}\frac{\beta I\,\Delta\vartheta}{2F} \\ & \quad = \left(E_{\text{cell}}(t) - E_{\text{thermoneutral,bath}}\right)I + Q_{\mathrm{f}}(t) + \Delta QH(t-t_1) - \Delta QH(t-t_2) \\ & \qquad - \frac{0.75I}{F}\left(\frac{P}{P^* - P}\right)\left(C_{P,\mathrm{D_2O,v}}\,\Delta\vartheta + L\right) \\ & \qquad - k^\circ_{\mathrm{R}}\vartheta^3_{\text{bath}}\left[1 - \frac{(1+\lambda)It}{2FM^\circ}\right]\left[\left[\frac{(\vartheta_{\text{bath}} + \Delta\vartheta)^4 - \vartheta^4_{\text{bath}}}{\vartheta^3_{\text{bath}}}\right] + 4\Phi\,\Delta\vartheta\right] \end{aligned} \tag{A3.9}$$

where $E_{\text{thermoneutral,bath}}$ (≈ 1.54 V) is the cell voltage at which the electrolysis is thermoneutral at the bath temperature. Equation (A3.9) is still difficult to apply in several important respects. In the first place, $Q_{\mathrm{f}}(t)$ is an unknown function of time and temperature. We have assumed here that these variations are sufficiently small so that Q_{f} can be regarded as a constant throughout any given measurement cycle; longer term objectives must clearly include the design of filters which will allow the measurement of Q_{f} in real time. Secondly, analytical solutions require further simplifications of eqn. (A3.9) and, in particular, the linearization of the heat transfer term (see Appendix 4). Thirdly, while the time dependence of the cell potential can be measured, the functional form cannot be predicted a priori and this too precludes the analytical integration of eqn. (A3.7) and complicates the numerical integration of the equation used in the non-linear regression procedure outlined in Appendix 5. Furthermore, since the vapor pressure is temperature dependent, the term $(0.75I/F)(P/(P^*-P))(C_{P,D_2O,v}\Delta\vartheta + L)$ is also a function of time. We note, however, that we can carry out a Taylor series expansion of this term as well as of all the component parts of $E_{\text{cell}}(t)$ (see eqn. A3.1) about a chosen origin in temperature, ϑ°. Since the variations in temperature are small, we are concerned only with the first derivatives and obtain

$$\begin{aligned} & \left\{\frac{\mathrm{d}E_{\text{cell}}}{\mathrm{d}\vartheta} + \frac{\mathrm{d}}{\mathrm{d}\vartheta}\left[\frac{0.75I}{F}\left(\frac{P}{P^* - P}\right)\left(C_{P,\mathrm{D_2O,v}}\,\Delta\vartheta + L\right)\right]\right\} I\,\Delta\vartheta' \\ & \quad = \left\{\frac{\Delta S^{\ominus}\vartheta^\circ}{2F} - \frac{\Delta H^{\neq}_{\text{anodic}}}{\beta F} + \eta^\circ_{\text{anodic}} - \frac{\Delta H^{\neq}_{\text{cathodic}}}{\alpha F} - \eta^\circ_{\text{cathodic}} - \frac{C\,\Delta H^{\neq}_{\kappa}}{\kappa^\circ R\vartheta^\circ}\right. \\ & \qquad \left. + \frac{0.75L}{F}\frac{L}{R\vartheta_0}\frac{P^\circ/P^*}{(1 - P^\circ/P^*)^2}\left(C_{P,\mathrm{D_2O,v}}\,\Delta\vartheta^\circ + L\right)\right\}\frac{I\,\Delta\vartheta'}{\vartheta^\circ} = \frac{\psi I}{\vartheta^\circ}\,\Delta\vartheta' \end{aligned} \tag{A3.10}$$

where

$$\Delta\vartheta' = \Delta\vartheta - \Delta\vartheta^\circ \qquad \text{(A3.11)}$$

Here, $\Delta S^{\ddagger}$ is the entropy change in reaction (i), $\Delta H^{\neq}_{anodic}$, $\Delta H^{\neq}_{cathodic}$, and $\Delta H_{\kappa}^{\ddagger}$ are the relevant activation energies, K is the conductance, C is a constant, α and β are transfer coefficients, and $\Delta\vartheta^\circ$ is the difference between the cell and thermostat temperatures at the chosen origin where the cell temperature is ϑ°. It can be seen that the magnitude (and even sign) of ψ is difficult to predict so that it is best to derive this as an empirical constant from the experimental observations. This procedure also has the advantage that it corrects automatically for other unquantified changes in the enthalpy input e.g. those due to changes in the concentration of electrolyte. Using eqn. (A3.10), we can cast eqn. (A3.9) into the tractable form

$$\begin{aligned} & C_{P,\mathrm{D_2O},\mathrm{l}}\left[M^\circ - \frac{(1+\beta)It}{2F}\right]\frac{\mathrm{d}\,\Delta\vartheta}{\mathrm{d}t} - C_{P,\mathrm{D_2O},\mathrm{l}}\frac{\beta I\,\Delta\vartheta}{2F} \\ & = \left(E^\circ_{\mathrm{cell}} - E_{\mathrm{thermoneutral,bath}} + \frac{\psi\,\Delta\vartheta'}{\vartheta^\circ}\right)I + Q_{\mathrm{f}}(t) + \Delta QH(t-t_1) - \Delta QH(t-t_2) \\ & \quad - \frac{0.75I}{F}\left(\frac{P^\circ}{P_0^* - P^\circ}\right)\left(C_{P,\mathrm{D_2O,v}}\,\Delta\vartheta^\circ + L\right) \\ & \quad - k^\circ_{\mathrm{R}}\vartheta^3_{\mathrm{bath}}\left[1 - \frac{(1+\lambda)It}{2FM^\circ}\right]\left[\left[\frac{(\vartheta_{\mathrm{bath}} + \Delta\vartheta)^4 - \vartheta^4_{\mathrm{bath}}}{\vartheta^3_{\mathrm{bath}}}\right] + 4\Phi\,\Delta\vartheta\right] \end{aligned} \qquad \text{(A3.12)}$$

Here E°_{cell} is the measured cell potential at a time chosen as the origin for measurements at which point the difference in temperature between the cell and bath is $\Delta\vartheta^\circ$. The simplified "black box" representation of eqn. (A3.12) is shown in Fig. A3.2.

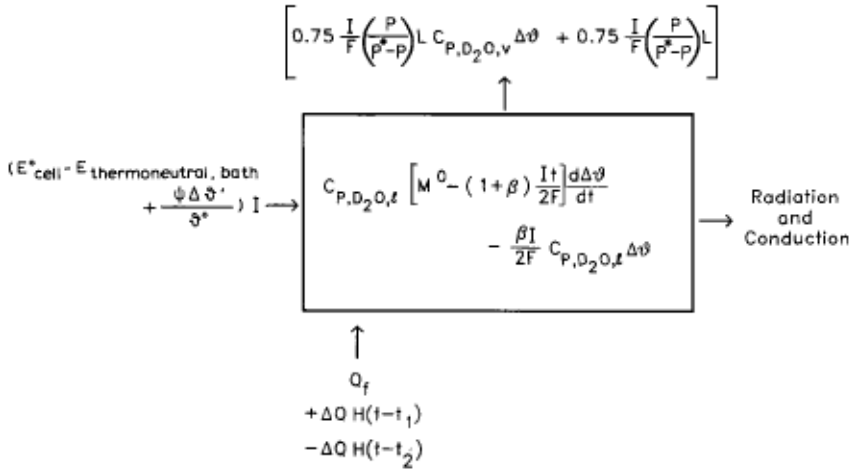

Fig. A3.2. Actual "black-box" representation of the heat flows in the Dewar calorimeters used in this work and taking into account $\gamma \approx 1$.

APPENDIX 4

Analytical solutions for the "black box" model: approximate evaluation of Q_f and of the heat transfer coefficients

As the differential equation (A3.9) governing the behavior of the "black box" model is inhomogeneous and non-linear, we need to make a number of approximations in order to achieve analytical solutions. In the first place we use the linearization of eqn. (A2.13) of the heat transfer term. Secondly, we write

$$Q = \left(E^{\circ}_{\text{cell}} - E_{\text{thermoneutral,bath}} - \frac{\psi \Delta\vartheta^{\circ}}{\vartheta^{\circ}} \right) I + Q_f - \frac{0.75I}{F} \left(\frac{P^{\circ}}{P_0^{*} - P^{\circ}} \right) \left(C_{P,\mathrm{D_2O,l}}\, \Delta\vartheta^{\circ} + L \right) \tag{A4.1}$$

and we regard this as being constant during any given measurement cycle. Thirdly we note that $\beta C_{P,D_2O,v} I \Delta\vartheta / 2F$ is a negligibly small quantity in comparison with the other terms in eqn. (A3.9). We first consider the solution in the absence of the resistive heating calibration term ΔQ and write eqn. (A3.9) in standard form

$$\frac{\mathrm{d}\,\Delta\vartheta}{\mathrm{d}t} = \frac{Q}{C_{P,\mathrm{D_2O,l}} M^{\circ}} \left[1 - \frac{(1+\beta) It}{2FM^{\circ}} \right]^{-1} - \frac{\left[4k''_{\mathrm{R}} \vartheta^{3}_{\text{bath}} - 4k''_{\mathrm{R}} \vartheta^{3}_{\text{bath}} \frac{(1+\lambda) It}{2FM^{\circ}} - \frac{\psi I}{\vartheta^{\circ}} \right]}{C_{P,\mathrm{D_2O,l}} M^{\circ}} \left[1 - \frac{(1+\beta) It}{2FM^{\circ}} \right]^{-1} \Delta\vartheta \tag{A4.2}$$

Furthermore, as $(1+\beta) It / 2FM^{\circ}$ is also small, we can expand eqn. (A4.2) to give

$$\frac{\mathrm{d}\,\Delta\vartheta}{\mathrm{d}t} + \frac{4k''_{\mathrm{R}} \vartheta^{3}_{\text{bath}}}{C_{P,\mathrm{D_2O,l}} M^{\circ}} \left[1 - \frac{\psi I}{4k''_{\mathrm{R}} \vartheta^{3}_{\text{bath}} \vartheta^{\circ}} - \frac{(\lambda - \beta) It}{2FM^{\circ}} \right] \Delta\vartheta = \frac{Q}{C_{P,\mathrm{D_2O,l}} M^{\circ}} \left[1 + \frac{(1+\beta) It}{2FM^{\circ}} \right] \tag{A4.3}$$

We write eqn. (A4.3) in the form

$$\frac{\mathrm{d}}{\mathrm{d}t} \left\{ \Delta\vartheta \exp \frac{4k''_{\mathrm{R}} \vartheta^{3}_{\text{bath}}}{C_{P,\mathrm{D_2O,l}} M^{\circ}} \left[\left(1 - \frac{\psi I}{4k''_{\mathrm{R}} \vartheta^{3}_{\text{bath}} \vartheta^{\circ}} \right) t - \frac{(\lambda - \beta) It^2}{4FM^{\circ}} \right] \right\} = \frac{Q}{C_{P,\mathrm{D_2O,l}} M^{\circ}} \left[1 + \frac{(1+\beta) It}{2FM^{\circ}} \right] \times \exp \frac{4k''_{\mathrm{R}} \vartheta^{3}_{\text{bath}}}{C_{P,\mathrm{D_2O,l}} M^{\circ}} \left[\left(1 - \frac{\psi I}{4k''_{\mathrm{R}} \vartheta^{3}_{\text{bath}} \vartheta^{\circ}} \right) t - \frac{(\lambda - \beta) It^2}{4FM^{\circ}} \right] \tag{A4.4}$$

The general integration of eqn. (A4.4) would itself have to be carried out numerically. However, we note that $k_R''\vartheta_{bath}^3(\lambda-\beta)It^2 / FC_{P,D_2O,l}M^{\circ 2}$ is a small quantity so that we can integrate eqn. (A4.4) to

$$\Delta\vartheta = Q\left[1-\frac{k_R''\vartheta_{bath}^3(\lambda-\beta)It^2}{FC_{P,D_2O,l}M^{\circ 2}}\right]^{-1}\left\{\frac{1}{\left(4k_R''\vartheta_{bath}^3-\frac{\psi I}{\vartheta^\circ}\right)}+\frac{(1+\beta)It}{2FM^\circ\left(4k_R''\vartheta_{bath}^3-\frac{\psi I}{\vartheta^\circ}\right)}\right.$$
$$-\frac{(1+\beta)IC_{P,D_2O,l}}{2F\left(4k_R''\vartheta_{bath}^3-\frac{\psi I}{\vartheta^\circ}\right)^2}-\frac{k_R''\vartheta_{bath}^3(\lambda-\beta)It^2}{FC_{P,D_2O,l}M^{\circ 2}\left(4k_R''\vartheta_{bath}^{\circ 3}-\frac{\psi I}{\vartheta^\circ}\right)}$$
$$\left.+\frac{2k_R''\vartheta_{bath}^3(\lambda-\beta)It}{FM^\circ\left(4k_R''\vartheta_{bath}^3-\frac{\psi I}{\vartheta^\circ}\right)^2}-\frac{2k_R''\vartheta_{bath}^3(\lambda-\beta)IC_{P,D_2O,l}}{F\left(4k_R''\vartheta_{bath}^3-\frac{\psi I}{\vartheta^\circ}\right)^3}\right\}$$
$$+\Delta\vartheta^\circ\left[1-\frac{k_R''\vartheta_{bath}^3(\lambda-\beta)It^2}{FC_{P,D_2O,l}M^{\circ 2}}\right]^{-1}\exp\left[-\left(4k_R''\vartheta_{bath}^3-\frac{\psi I}{\vartheta^\circ}\right)\right]\frac{t}{C_{P,D_2O,l}M^\circ}$$
$$-Q\left[1-\frac{k_R''\vartheta_{bath}^3(\lambda-\beta)It^2}{FC_{P,D_2O,l}M^{\circ 2}}\right]^{-1}$$
$$\times\left\{\frac{1}{\left(4k_R''\vartheta_{bath}^3-\frac{\psi I}{\vartheta^\circ}\right)}-\frac{(1+\beta)IC_{P,D_2O,l}}{2F\left(4k_R''\vartheta_{bath}^3-\frac{\psi I}{\vartheta^\circ}\right)^2}\right.$$
$$\left.-\frac{2k_R''\vartheta_{bath}^3(\lambda-\beta)IC_{P,D_2O,l}}{F\left(4k_R''\vartheta_{bath}^3-\frac{\psi I}{\vartheta^\circ}\right)^3}\right\}\exp\left[-\left(4k_R''\vartheta_{bath}^3-\frac{\psi I}{\vartheta^\circ}\right)\right]\frac{t}{C_{P,D_2O,l}M^\circ} \tag{A4.5}$$

where we have also taken into account the initial condition

$$\Delta\vartheta = \Delta\vartheta^\circ, \quad t=0 \tag{A4.6}$$

It can be seen that, in addition to the linear and quadratic terms in eqn. (A4.5), the time dependence of the system is controlled by a relaxation time

$$\tau = \frac{C_{P,D_2O,l}M^\circ}{\left(4k_R''\vartheta_{bath}^3-\frac{\psi I}{\vartheta^\circ}\right)} \tag{A4.7}$$

For the calorimeters used here, $\tau \cong 1600\,\mathrm{s}$. In the analysis of the data using algebraic solutions we are interested principally in the behavior of eqn. (A4.5) at long times. Taking into account also that $k_R''\vartheta_{bath}^3(\lambda-\beta)It^2/FC_{P,D_2O,l}M^{\circ 2} \ll 1$, $\beta < \lambda$ and $\psi I/\vartheta^\circ < 4k_R''\vartheta_{bath}^3$, we obtain

$\beta < \lambda$, and $\psi I/\vartheta^\circ < 4k_R''\vartheta_{bath}^3$, we obtain

$$\Delta\vartheta \cong \frac{Q}{\left(4k_R''\vartheta_{bath}^3 - \frac{\psi I}{\vartheta^\circ}\right)} + \frac{Q(1+\lambda)It}{2FM^\circ\left(4_R''\vartheta_{bath}^3 - \frac{\psi I}{\vartheta^\circ}\right)} - \frac{Q(1+\lambda)IC_{P.D_2O.l}}{2F\left(4k_R''\vartheta_{bath}^3 - \frac{\psi I}{\vartheta^\circ}\right)^2}$$

$$\cong \frac{Q}{\left(4k_R''\vartheta_{bath}^3 - \frac{\psi I}{\vartheta^\circ}\right)} + \frac{Q(1+\lambda)It}{2FM^\circ\left(4k_R''\vartheta_{bath}^3 - \frac{\psi I}{\vartheta^\circ}\right)} \qquad \text{(A4.8)}$$

Since $(1+\lambda)C_{P,D_2O,l}/2F\left(4k_R''\vartheta_{bath}^3 - \psi I/\vartheta^\circ\right) \ll 1$. We note that the quadratic time dependent terms in eqn. (A4.5) cancel at this level of approximation and that eqn. (A4.8) predicts the linear increase of ϑ with *t* observed at long times (see also further below). The most important conclusion is that heat transfer takes place with the modified heat transfer coefficient $4k_R''\vartheta_{bath}^3 - \psi I/\vartheta^\circ$ rather than with the value $4k_R''\vartheta_{bath}^3$. This is due to the fact that the temperature-time dependence automatically takes into account the change in the input enthalpy as expressed by eqn. (A3.10). The effects of the progressive electrolysis of the contents of the Dewar calorimeter also follow from eqn. (A4.8) which can be written to a close approximation as

$$\Delta\vartheta \cong \frac{Q}{\left(4k_R''\vartheta_{bath}^3 - \frac{\psi I}{\vartheta^\circ}\right)\left(1 - \frac{(1+\lambda)It}{2FM^\circ}\right)} \qquad \text{(A4.9)}$$

Equation (A4.9) shows that the behavior of the system can be modelled by a linear decrease of the effective heat transfer coefficient with time.

We consider next the application of a resistive heating term ΔQ at a time $t = t_1$ at which the behavior of eqn. (A4.8) has been established, giving an initial condition

$$\Delta\vartheta = \frac{Q}{\left(4k_R''\vartheta_{bath}^3 - \frac{\psi I}{\vartheta^\circ}\right)} + \frac{Q(1+\lambda)It_1}{2FM^\circ\left(4k_R''\vartheta_{bath}^3 - \frac{\psi I}{\vartheta^\circ}\right)} \qquad \text{(A4.10)}$$

As for the case discussed above, this initial condition does not affect the long time asymptotic variation of ϑ which is given at the same level of approximation by

$$\Delta\vartheta + \Delta\Delta\vartheta = \frac{(Q+\Delta Q)}{\left(4k_R''\vartheta_{bath}^3 - \frac{\psi I}{\vartheta^\circ}\right)} + \frac{(Q+\Delta Q)(1+\lambda)It}{2FM^\circ\left(4k_R''\vartheta_{bath}^3 - \frac{\psi I}{\vartheta^3}\right)} \qquad \text{(A4.11)}$$

The shift in temperature above the sloping base line (eqn. A4.8) is given by

$$\Delta\Delta\vartheta = \frac{\Delta Q}{\left(4k''_{\mathrm{R}}\vartheta^{3}_{\mathrm{bath}} - \frac{\psi I}{\vartheta^{\circ}}\right)} + \frac{\Delta Q(1+\lambda)It}{2FM^{\circ}\left(4k''_{\mathrm{R}}\vartheta^{3}_{\mathrm{bath}} - \frac{\psi I}{\vartheta^{\circ}}\right)}$$

$$\cong \frac{\Delta Q}{\left(4k''_{\mathrm{R}}\vartheta^{3}_{\mathrm{bath}} - \frac{\psi I}{\vartheta^{\circ}}\right)\left(1 - \frac{(1+\lambda)It}{2FM^{\circ}}\right)} \qquad \text{(A4.12)}$$

and it follows that the heat transfer coefficient required for the calculation of the total heat output is precisely that determined from the application of the resistive joule heating term ΔQ. Optimum accuracy will be achieved in the application of these algebraic expressions if the evaluations are made at the end of the resistive heating input cycle, Fig. A4.1.

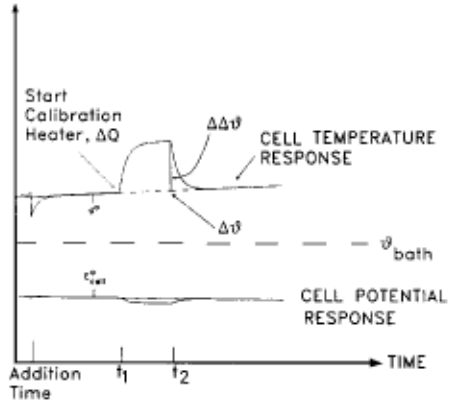

Fig. A4.1. Diagram of the method of experimental determination of approximate heat flow in the Dewar calorimeter, including the response $\Delta\Delta\vartheta$ for application of the calibration pulse ΔQ.

It should be noted that the effects of changes in the electrical input energy to the cell (due to variations in the cell potential with time) are automatically taken into account through eqn. (A3.10) in the prediction of the temperature-time plots. In consequence, the derived heat transfer coefficients allow for these changes in electrical input energy (the term $\psi I / \vartheta^{\circ}$). In these evaluations, the cell potential must be regarded as being constant and given by the value at the chosen time origin and the value of Q must not be corrected for any variation of the potential with time as, otherwise, these effects would be counted twice.

APPENDIX 5

Data evaluation: non-linear regression fitting of the "black-box" models of the calorimeter to the experimental data

It has been shown that the differential equation (A3.7) governing the behavior of the "black-box" model of the calorimeter can be expressed accurately by eqn. (A3.11). The general integration of this equation must be carried out numerically in view of its non-linearity and inhomogeneity. At the *n*th time interval we have

$$\left(\frac{\mathrm{d}\,\Delta\vartheta}{\mathrm{d}t}\right)_n = \left\{\left(E_{\mathrm{cell},t=0} + \frac{\psi\,\Delta\vartheta_n'}{\vartheta^\circ} - E_{\mathrm{thermoneutral,bath}}\right) I + Q_f + \Delta QH(t-t_1) - \Delta QH(t-t_2) - \frac{k_R'\vartheta_{\mathrm{bath}}^3\left[1-\frac{(1+\lambda)I(n\,\Delta t)}{2FM^\circ}\right]\left[\frac{(\vartheta_{\mathrm{bath}}+\Delta\vartheta_n)^4-\vartheta_{\mathrm{bath}}^4}{\vartheta_{\mathrm{bath}}^3}\right]}{C_{P,\mathrm{D_2O},l}M^\circ\left[1-\frac{(1+\beta)I(n\,\Delta t)}{2FM^\circ}\right]}\right\} \tag{A5.1}$$

where we have used the approximation of eqn. (A2.9) in formulating the heat transfer term. Forward integration is carried out by using

$$\Delta\vartheta_{n+1} = \Delta\vartheta_n + \left(\frac{\mathrm{d}\,\Delta\vartheta}{\mathrm{d}t}\right)_n \Delta t \tag{A5.2}$$

We use these calculated values to form

$$\chi^2 = \sum_{n=1}^{N} \frac{\left(\Delta\vartheta_{n,\mathrm{exp}} - \Delta\vartheta_{n,\mathrm{calc}}\right)^2}{\sigma_n^2} \tag{A5.3}$$

where N is the number of data points and we take σ_n^2 as

$$\sigma_n^2 = \frac{10^{-4}}{\left(\Delta\vartheta_{n,\mathrm{exp}}\right)^2} \tag{A5.4}$$

In view of the magnitudes of the curvatures of the parameter space hypersurfaces, it is convenient to define the independent parameters as

$$\beta_1 = \frac{(E_{\text{cell},t=0} - E_{\text{thermoneutral,bath}})I + Q_f}{C_{P,\text{D}_2\text{O},l} M^\circ} \tag{A5.5}$$

$$\beta_2 = \frac{\psi I}{C_{P,\text{D}_2\text{O},l} M^\circ \vartheta^\circ} \tag{A5.6}$$

$$\beta_3 = \frac{(1+\lambda)I}{2FM^\circ} \tag{A5.7}$$

$$\beta_4 = \frac{k'_R \vartheta^3_{\text{bath}}}{C_{P,\text{D}_2\text{O},l} M^\circ} \tag{A5.8}$$

$$\beta_5 = M^\circ \tag{A5.9}$$

Using eqns. (A5.5)-(A5.9), we can write eqn. (A5.1) as

$$\left(\frac{\text{d}\,\Delta\vartheta}{\text{d}t}\right)_n = \frac{\beta_1 + \beta_2\,\Delta\vartheta'_n - \beta_4[1-\beta_3(n\,\Delta t)]\left[\dfrac{(\vartheta_{\text{bath}} + \Delta\vartheta_n)^4 - \vartheta^4_{\text{bath}}}{\vartheta^3_{\text{bath}}}\right]}{1 - \dfrac{(1+\beta)I(n\,\Delta t)}{2F\beta_5}} + \frac{(\Delta Q)}{C_{P,\text{D}_2\text{O},l}\beta_5 - \dfrac{(1+\beta)C_{P,\text{D}_2\text{O},l} I(n\,\Delta t)}{2F}} \tag{A5.10}$$

We take the differentials of $\left(d\ \Delta\vartheta / dt\right)_n$ with respect to the parameters given in eqns. (A5.5)-(A5.9):

$$\alpha_1 = \frac{\partial}{\partial\beta_1}\left(\frac{\mathrm{d}\ \Delta\vartheta}{\mathrm{d}t}\right)_n = \frac{1}{1 - \dfrac{(1+\beta)I(n\ \Delta t)}{2F\beta_5}} \tag{A5.11}$$

$$\alpha_2 = \frac{\partial}{\partial\beta_2}\left(\frac{\mathrm{d}\ \Delta\vartheta}{\mathrm{d}t}\right)_n = \frac{\Delta\vartheta_n'}{1 - \dfrac{(1+\beta)I(n\ \Delta t)}{2F\beta_5}} \tag{A5.12}$$

$$\alpha_3 = \frac{\partial}{\partial\beta_3}\left(\frac{\mathrm{d}\ \Delta\vartheta}{\mathrm{d}t}\right)_n = \frac{\beta_4(n\ \Delta t)\left[\dfrac{(\vartheta_{\mathrm{bath}} + \Delta\vartheta_n)^4 - \vartheta_{\mathrm{bath}}^4}{\vartheta_{\mathrm{bath}}^3}\right]}{1 - \dfrac{(1+\beta)I(n\ \Delta t)}{2F\beta_5}} \tag{A5.13}$$

$$\alpha_4 = \frac{\partial}{\partial\beta_4}\left(\frac{\mathrm{d}\Delta\vartheta}{\mathrm{d}t}\right)_n = \frac{-\left[1 - \beta_3(n\ \Delta t)\right]\left[\dfrac{(\vartheta_{\mathrm{bath}} + \Delta\vartheta_n)^4 - \vartheta_{\mathrm{bath}}^4}{\vartheta_{\mathrm{bath}}^3}\right]}{1 - \dfrac{(1+\beta)I(n\ \Delta t)}{2F\beta_5}} \tag{A5.14}$$

$$\begin{aligned}\alpha_5 &= \frac{\partial}{\partial\beta_5}\left(\frac{\mathrm{d}\ \Delta\vartheta}{\mathrm{d}t}\right)_n \\ &= \frac{-\left\{\beta_1 + \beta_2\ \Delta\vartheta_n' - \beta_4[1 - \beta_3 n\ \Delta t]\left[\dfrac{(\vartheta_{\mathrm{bath}} + \Delta\vartheta_n)^4 - \vartheta_{\mathrm{bath}}^4}{\vartheta_{\mathrm{bath}}^3}\right]\right\}\dfrac{(1+\beta)I(n\ \Delta t)}{2F\beta_5^2}}{\left[1 - \dfrac{(1+\beta)I(n\ \Delta t)}{2F\beta_5}\right]^2} \\ &\quad - \frac{(\Delta Q)}{C_{P,\mathrm{D_2O,l}}\left[\beta_5 - \dfrac{(1+\beta)C_{P,\mathrm{D_2O,l}}I(n\ \Delta t)}{2F}\right]^2}\end{aligned} \tag{A5.15}$$

We now express the differential $\left(d\ \Delta\vartheta / dt\right)_n$ in terms of the value $\left(d\ \Delta\vartheta / dt\right)_{n,0}$ obtained with a given set of the parameters $\beta_{1.0} - \beta_{5.0}$ and the sum of the perturbations of $\left(d\ \Delta\vartheta / dt\right)_n$ due to the variations of $\delta\beta_j$ of the parameters $\beta_1 - \beta_5$:

$$\left(\frac{\mathrm{d}\,\Delta\vartheta}{\mathrm{d}t}\right)_n = \left(\frac{\mathrm{d}\,\Delta\vartheta}{\mathrm{d}t}\right)_{n,0} + \sum_{j=1}^{5} \alpha_j \delta\beta_j \qquad \text{(A5.16)}$$

We use eqn. (A5.16) in eqn. (A5.2) to estimate $\Delta\vartheta_{n+1}$

$$\Delta\vartheta_{n+1} = \Delta\vartheta_n + \left(\frac{\mathrm{d}\,\Delta\vartheta}{\mathrm{d}t}\right)_{n,0} \Delta t + \sum_{j=1}^{5} \alpha_j \delta\beta_j\, \Delta t \qquad \text{(A5.17)}$$

and, in turn, use eqn. (A5.17) to form χ^2:

$$\chi^2 = \sum_{n=1}^{N} \frac{1}{\sigma_n^2} \left\{ \Delta\vartheta_{n,\mathrm{exp}} - \Delta\vartheta_0 - \sum_{k=1}^{n} \left(\frac{\mathrm{d}\,\Delta\vartheta}{\mathrm{d}t}\right)_{k,0} \Delta t - \sum_{k=1}^{n} \sum_{j=1}^{5} \alpha_j \delta\beta_j\, \Delta t \right\}^2 \qquad \text{(A5.18)}$$

Here, $\Delta\vartheta_0$ is the value of the difference between the cell and bath temperatures at the time $t = 0$, chosen as the origin for the evaluation of the parameters of eqns. (A5.5)-(A5.9). Minimization of χ^2 with respect to the parameters gives the set of equations

$$\frac{\partial\chi^2}{\partial(\beta_i)} = -2 \sum_{n=1}^{N} \frac{1}{\sigma_n^2} \left\{ \Delta\vartheta_{n,\mathrm{exp}} - \Delta\vartheta_0 - \sum_{k=1}^{n} \left(\frac{\mathrm{d}\,\Delta\vartheta}{\mathrm{d}t}\right)_{k,0} \Delta t - \sum_{k=1}^{n} \sum_{j=1}^{5} \alpha_j \delta\beta_j\, \Delta t \right\} \sum_{k=1}^{n} \alpha_i\, \Delta t \qquad \text{(A5.19)}$$

With

$$\Gamma_{i,0} = \sum_{n=1}^{N} \frac{1}{\sigma_n^2} \left\{ \Delta\vartheta_{n,\mathrm{exp}} - \Delta\vartheta_0 - \sum_{k=1}^{n} \left(\frac{\mathrm{d}\,\Delta\vartheta}{\mathrm{d}t}\right)_{k,0} \Delta t \right\} \sum_{k=1}^{n} \alpha_i\, \Delta t \qquad \text{(A5.20)}$$

and

$$\Lambda_{i,j} = \sum_{n=1}^{N} \frac{1}{\sigma_n^2} \sum_{k=1}^{n} \alpha_i\, \Delta t \sum_{k=1}^{n} \alpha_j\, \Delta t \qquad \text{(A5.21)}$$

we can write eqn. (A5.19) in the usual matrix form

$$\Lambda_{i,j} \delta\beta_j = \Gamma_{i,0} \qquad \text{(A5.22)}$$

Inversion gives the values of $\delta\beta$ which we use to define a new set of starting values of the β_i, namely $\beta_{i,0} + \delta\beta_i$. We iterate until the set β_i as well as χ^2 have converged adequately and then derive the variances of the parameters

$$\sigma_{\beta_i}^2 = \epsilon_{i,i} \qquad \text{(A5.23)}$$

to a close approximation from an angles of the error matrix

$$\epsilon_{i,j} = \Lambda_{i,j}^{-1} \qquad \text{(A5.24)}$$

In carrying out this fitting procedure, it is convenient to use the parameters derived by applying the approximate equations (A4.9) and (A4.12) or, more exactly, eqns. (A2.9) and (A2.10) as the initial values, since these parameters are already close to the "best" values. Furthermore it is convenient (though not essential) to derive the value of $\psi I / C_{P,D_2O,1} M^\circ \vartheta^\circ$ by first fitting data of E_{cell} versus $\Delta\vartheta$ using linear regression. By using this procedure, the optimization is reduced to 4 parameters and the sensitivity of the calculation to β_5 is greatly increased, thereby speeding the calculation.

We have used a Marquardt-type algorithm throughout this work in which the diagonal elements of the matrix $\Lambda_{i,j}$ are scaled appropriately so as to follow either a path of steepest descent or along the directions of the parameter space as required to optimize the reduction of χ^2. The calculation has been demonstrated for one particular model of the "black box" but the changes required for the modifications of the model will be self-evident. Programs for implementing the fitting procedures are available on request. The analysis presented here has applications in the general field of numerical analysis which will be discussed elsewhere.

APPENDIX 6

Some comments on the data contained in the preliminary publication [1,2]

Table A6.1 gives the essential experimental and derived information for the experiments on rod electrodes which were previously reported [1,2] in a similar form to that of Tables 3 and 4 of the main text of the present paper. Columns 4 and 5 of Table A6.1 follow immediately from Tables 1 and 2 of the preliminary publication using

total Joule heat input

$$= \frac{100 \times \text{excess Joule heat input}}{\%\ \text{of break even based on Joule heat input to cell for reaction}} \qquad \text{(A6.1)}$$

and

$$E_{cell} = \frac{\text{total Joule heat input}}{\text{cell current}} + 1.54 \qquad \text{(A6.2)}$$

Alternatively, the cell voltage may be calculated from

$$E_{cell} = \frac{\text{total Joule heat input}}{\%\ \text{of breakeven based on total energy input to cell for reaction (i)} \times \text{cell current}} \qquad \text{(A6.3)}$$

In practice, the derived data which were presented in Tables 1 and 2 of the preliminary paper [1,2] were naturally obtained by applying eqns. (A6.1), (A6.2) and (A6.3) so as to give the percentage of break even values based on cell reaction (i). It was evidently difficult for readers to reconstruct the primary information from the Tables in the preliminary publication; readers also found it difficult to accept the validity of the arguments underlying the calculation of the percentage of break even based on an anode reaction

$$D_2 + 2\ OD^- \rightarrow 2\ D_2O + 4e^- \qquad \text{(A6.i)}$$

rather than on that used in the actual experiment

$$4\ OD^- \rightarrow 2\ D_2O + O_2 + 4\ e^- \qquad \text{(A6.ii)}$$

We point out here that a practical working system would never be based on the conditions used in obtaining the data given in Tables 4 and A6.1 and that statements made on the percentage of excess enthalpy relative to the enthalpy or energy input to the cell are arbitrary since they depend on the cell design, concentration of the electrolyte, etc. It is better therefore to base projections of the efficiency of the system on the fuel cell anode reaction (A6.i) which would almost certainly be used in practical systems and on likely values of the cell voltage which would apply to such cells which would be operated with minimum interelectrode gaps and at high electrolyte concentrations. These considerations underlay the calculation of column (c) of Table 2 of the preliminary paper (with amendments in ref. 2).

TABLE A6.1

Excess enthalpy observed for 0.1, 0,2, and 0.4 cm diameter palladium rods as a function of current density. Values of Q_{excess} derived using an approximate method of data analysis only

Electrode Dimensions (diameter × length) /cm	Batch[a] and electrolyte[b]	Current density [c] /mA cm^{-2}	E_{cell} /V	Q_{input} /W	Q_{input} /W	Q_{excess} /W	Specific Q_{excess} /W cm^{-3}	Q_{excess} /% of break even [d]	[e]
0.1 × 10	1, ○	8 (25)	2.754	0.0304	0.0379	0.0075	0.095	25 (23)	11 (12)
0.1 × 10	1, ○	64 (200)	3.602	0.412	0.481	0.079	1.01	19	11
0.1 × 1.25	1, ○	512 (200)	8.995	1.491	1.573	0.082	8.33	5	4 (5)
0.2 × 10	1, □	8 (50)	2.702	0.058	0.094	0.036	0.115	62	27
0.2 × 10	1, □	64 (400)	4.231	1.07	1.57	0.493	1.57	46	29
0.2 × 1.25	1, □	512 (400)	8.461	2.77	3.15	0.378	9.61	14	11
0.4 × 10	1, △	8 (100)	2.91	0.137	0.29	0.153	0.122	112 (111)	53
0.4 × 10	1, △	64 (800)	4.86	2.66	4.41	1.75	1.39	66	45
0.4 × 1.25	1, △	512 (800)	8.655	5.69	9.04	3.35	21.4	59	48

[a] All rods were from Batch 1.
[b] 0.1 M LiOD. All measurements were made in the same batch of D_2O of 99.9% isotopic purity.
[c] values in parentheses: actual applied currents.
[d] Excess heating expressed as a percentage of the enthalpy input to the cell.
[e] Excess heating expressed as a percentage of the energy input to the cell. The values in parentheses in columns [d] and [e] were given in Table 2 of ref. 1.

GLOSSARY OF SYMBOLS USED

Q_i'	Approximate rate of steady state heat generation at a given temperature, W.
Q_f	Rate of generation of excess enthalpy, W.
$Q_f(t)$	Time dependent rate of generation of excess enthalpy, W.
r	Shortest eddy decay length, cm.
t	Time, s.
v	Symbol for vapor phase.
V	Volume, cm^3.
W	Fluctuating enthalpy content, J.
α_i	Differentials of the time rate change of temperature equation with respect to the system parameters β_i
β	Dimensionless term allowing for more rapid time dependent decrease of water equivalent of cell than that expected from electrolysis alone.
β_i	Parameters of the "black-box" representation of the calorimeter.
γ	Current efficiency of electrolysis toward a given reaction.
$\Gamma_{i,0}$	Elements of the weighted deviation vector for the matrix equation used in the non-linear regression fitting algorithm.
$\Delta G^{\ominus}$	Standard Gibbs energy change, J mol^{-1}.
$\Delta H^{\ominus}$	Standard enthalpy change, J mol^{-1}.
$\Delta H_i^{\neq}$	Activation energy, J mol^{-1}.
ΔQ	Rate of heat dissipation of calibration heater, W.
$\Delta S^{\ominus}$	Standard free entropy change, J K^{-1} mol^{-1}.
$\delta\beta_i$	Variations in the parameters of the "black-box" representation of the calorimeter.
$\delta\vartheta$	Incremental temperature change, K.
$\delta\vartheta_i$	Incremental temperature change across glass walls of cell, K.
$\delta\vartheta\vartheta_i$	Additional temperature change across glass walls due to additional enthalpy input to cell, K.
$\Delta\vartheta$	Difference in cell and bath temperature, K.
$\Delta\vartheta'$	Difference in cell and bath make-up stream temperature, K.
$\Delta\vartheta'$	Difference between the cell temperature at a given time and that at a chosen time origin, K.
$\Delta\vartheta_i$	Difference in cell and bath temperature at a given rate of enthalpy release, K.
$\Delta\vartheta_n$	Difference in cell and bath temperature at the nth time interval, K.
$\Delta\vartheta_{n,\mathrm{exp}}$	Difference in experimental cell and bath temperature at the nth time interval, K.
$\Delta\vartheta_{n,\mathrm{calc}}$	Calculated difference in cell and bath temperature at the nth time interval, K.
$\Delta\Delta\vartheta_i$	Temperature rise in cell due to application of a calibration pulse of heat, K.
$\epsilon_{i,j}$	Elements of the error matrix for the parameters determined by the non-linear regression fitting algorithm.

Q_i'	Approximate rate of steady state heat generation at a given temperature, W.
Q_f	Rate of generation of excess enthalpy, W.
$Q_f(t)$	Time dependent rate of generation of excess enthalpy, W.
r	Shortest eddy decay length, cm.
t	Time, s.
v	Symbol for vapor phase.
V	Volume, cm^3.
W	Fluctuating enthalpy content, J.
α_i	Differentials of the time rate change of temperature equation with respect to the system parameters β_i
β	Dimensionless term allowing for more rapid time dependent decrease of water equivalent of cell than that expected from electrolysis alone.
β_i	Parameters of the "black-box" representation of the calorimeter.
γ	Current efficiency of electrolysis toward a given reaction.
$\Gamma_{i,0}$	Elements of the weighted deviation vector for the matrix equation used in the non-linear regression fitting algorithm.
$\Delta G^{\ominus}$	Standard Gibbs energy change, J mol^{-1}.
$\Delta H^{\ominus}$	Standard enthalpy change, J mol^{-1}.
$\Delta H_i^{\neq}$	Activation energy, J mol^{-1}.
ΔQ	Rate of heat dissipation of calibration heater, W.
$\Delta S^{\ominus}$	Standard free entropy change, J K^{-1} mol^{-1}.
$\delta\beta_i$	Variations in the parameters of the "black-box" representation of the calorimeter.
$\delta\vartheta$	Incremental temperature change, K.
$\delta\vartheta_i$	Incremental temperature change across glass walls of cell, K.
$\delta\vartheta\vartheta_i$	Additional temperature change across glass walls due to additional enthalpy input to cell, K.
$\Delta\vartheta$	Difference in cell and bath temperature, K.
$\Delta\vartheta'$	Difference in cell and bath make-up stream temperature, K.
$\Delta\vartheta'$	Difference between the cell temperature at a given time and that at a chosen time origin, K.
$\Delta\vartheta_i$	Difference in cell and bath temperature at a given rate of enthalpy release, K.
$\Delta\vartheta_n$	Difference in cell and bath temperature at the nth time interval, K.
$\Delta\vartheta_{n,\mathrm{exp}}$	Difference in experimental cell and bath temperature at the nth time interval, K.
$\Delta\vartheta_{n,\mathrm{calc}}$	Calculated difference in cell and bath temperature at the nth time interval, K.
$\Delta\Delta\vartheta_i$	Temperature rise in cell due to application of a calibration pulse of heat, K.
$\epsilon_{i,j}$	Elements of the error matrix for the parameters determined by the non-linear regression fitting algorithm.

η_i	Overpotential for a given reaction, V.
ϑ_{bath}	Bath temperature, K.
$\vartheta_{\text{cell, } i}$	Cell temperature at a given rate of enthalpy release, K.
ϑ°	Cell temperature at $t = 0$, K.
κ	Conductance, S.
λ	Dimensionless parameter determining the more rapid decrease of the radiant surface area than would be predicted by electrolysis alone.
$\Gamma_{i,j}$	Elements of the matrix of coefficients of the parameter deviations for the matrix equation used in the non-linear regression fitting algorithm.
ν_i	Stoichiometric coefficients.
ρ_{D_2O}	Density of D_2O, g cm^{-3}.
σ_n	Sample standard deviation of a given temperature measurement, K.
$\sigma^2_{\beta_i}$	Variance of the values of the "best fit" parameters determined by the non-linear regression fitting algorithm.
τ	Characteristic relaxation time, s.
Φ	Proportionality constant relating conductive heat transfer to the radiative heat transfer term.
Φ	Autocorrelation function of enthalpy content, J^2.
χ^2	Sum of inverse variance weighted deviations between experimental data and values predicted by the model using the non-linear regression fitting algorithm.
ψ	Parameter determining the change of cell potential with temperature, V.
ω	Frequency, s^{-1}.

REFERENCES

1. M. Fleischmann, S. Pons and M. Hawkins, J. Electroanal. Chem., 261 (1989) 301.
2. M. Fleischmann, S. Pons and M. Hawkins, J. Electroanal. Chem., 263 (1989) 187.
3. R.C. Kainthla, M. Sklarczyk, L. Kaba, G.H. Lin, 0. Velev, N.J.C. Packham, J.C. Wass and J.O'M. Bockris, Int. J. Hydrogen Energy, 14 (1989) 771.
4. M.L. Oliphant, P. Harteck and Lord Rutherford, Nature, 133 (1934) 413.
5. N.J.C. Packham, K.L. Wolf, J.C. Wass, R.C. Kainthla and J.O'M. Bockris, J. Electroanal. Chem., 270 (1989) 451.
6. K.L. Wolf, N.J.C. Packham, D. Lawson, J. Shoemaker, F. Cheng, and J.C. Wass, Proceedings of the Workshop on Cold Fusion Phenomena, Santa Fe, NM, 23-25 May 1989; Fusion Technol., submitted.
7. E. Storms and C. Talcott, Proceedings of the Workshop on Cold Fusion Phenomena, Santa Fe, NM, 23-25 May 1989.

8. P.K. Iyengar, Fifth International Conference on Emerging Nuclear Energy Systems, Kae, 3-6 July 1989.
9. M.S. Krishnan, S.K. Malhotra, D.G. Gaonkar, M. Srinivasan, S.K. Sikka, A. Shyam, V. Chitra, T.S. Iyengar and P.K. Iyengar, Fusion Technol., submitted.
M.G. Nayar, S.K. Mitra, P. Raghunathan, M.S. Krishnan, S.K. Malhotra, D.G. Gaonkar, S.K. Sikka, A. Shyam and V. Chitra, Fusion Technol., submitted.

T.P. Radhakrishnan, R. Sundaresan, S. Gangadharan, B.K. Sen and T.S. Murthy, Fusion Technol., submitted.

G. Venkateswaran, P.N. Moorthy, K.S. Venkateswarlu, S.N. Guha, B. Yuvaraju, T. Datta, T.S.

Iyengar, M.S. Panajkar, K.A. Rao and K. Kishore, Fusion Technol., submitted.

T.S. Murthy, T.S. Iyengar, B.K. Sen and T.B. Joseph, Fusion Technol., submitted.

S.K. Malhotra, M.S. Krishnan and H.K. Sadhukhan, Fusion Technol., submitted.

R.K. Rout, M. Srinivasan and A. Shyam, Fusion Technol., submitted.

10. R. Gozzi, Proceedings of the Workshop on Cold Fusion Phenomena, Santa Fe, NM, 23-25 May 1989.
R. Zhou, Proceedings of the Workshop on Cold Fusion Phenomena, Santa Fe, NM, 23-25 May 1989.

D.P. Hutchinson, C.A. Bennett, R.K. Richards, J. Bullock IV and G. Powell, Oak Ridge National

Laboratory, Oak Ridge, TN, Technical Manuscript.

M.E. Wadsworth, S. Guruswamy, J.G. Byrne and J. Li, to be submitted.

M. McKubre, P. Searson, S. Smedley and F. Tanzella, in preparation.

Y. Arata and Y. Zhang, submitted.

A. Belzner, U. Bischler, S. Crouch-Baker, T.M. Guir, G. Lucier, M. Schreiber, and R.A. Huggins, Proceedings of the Workshop on Cold Fusion Phenomena, Santa Fe, NM, 23-25 May 1989.

A. Belzner, U. Bischler, S. Crouch-Baker, T.M. GUr, G. Lucier, M. Schreiber and R.A. Huggins, J. Fusion Energy, submitted.

R.C. Kainthla, 0. Velev, L. Kaba, G.H. Lin, N.J.C. Packham, M. Szklarczyk, J. Wass and J.O'M.

Bockris, Electrochim. Acta, 34 (1989) 1315.

D. Lewis and K. Sk6ld, Cold Fusion Session, 40th Meeting of the International Society of Electrochemistry, Kyoto, 11-18 September 1989.

N. Oyama, T. Ohsaka, 0. Hatozaki, N. Yamamoto, Y. Kurasawa, S. Kasahara, S. Takeoka, Y. Imai, Y. Oyama, T. Nakamura, T. Shibata and M. Imamura, Cold Fusion Session, 40th Meeting of the International Society of Electrochemistry, Kyoto, 11-18 September 1989.

A.J. Appleby, S. Srinivasan, Y.J. Kim, O.J. Murphy and C.R. Martin, Proceedings of the Workshop on Cold Fusion Phenomena, Santa Fe, NM, 23-25 May 1989.

J.O'M. Bockris, K. Wolf, R.C. Kainthla, 0. Velev and N.J.C. Packham, Cold Fusion Session, 40th Meeting of the International Society of Electrochemistry, Kyoto, 11-18 September 1989.

T.P. Radhakrishnan, R. Sundaresan, J. Arunachalam, V. Sitaramaraju, R. Kalyanaraman, S. Gangaharan and P.K. Iyengar, Fusion Technol., submitted.

V.C. Noninski and C.I. Noninski, submitted.

H. Bose, L.H. Prabhu, S. Sankaranarayanan, R.S. Shetiya, N. Veeraraghavan, P.V. Joshi, T.S. Murthy, B.K. Sen and K.G.B. Sharma, Fusion Technol., submitted.

C.D. Scott, J.E. Mrochek, E. Newman, T.C. Scott, G.E. Michaels and M. Petek, Oak Ridge National Laboratory, Oak Ridge, TN, Technical Manuscript 11322.

G.J. Schoessow, private communication, 1990.

A.J. Appleby, Y.J. Kim, O.J. Murphy and S. Srinivasan, 176th Meeting of the Electrochemical Society, Hollywood, FL, October 1989.

R. Adzic, DF. Gervasio, I. Bae, B. Cahan and E. Yeager, 176th Meeting of the Electrochemical Society, Hollywood, FL, October 1989.

U. Landau, W.M. Lynes, D. Roha, R. Saini and S. Rochel-Landau, 176th Meeting of the Electrochemical Society, Hollywood, FL, October 1989.

S. Crouch-Baker, T.M. Gur, G. Lucier, M. Schreiber and R.A. Huggins, 176th Meeting of the Electrochemical Society, Hollywood, FL, October 1989.

M.C.H. McKubre, S.I. Smedley, F.L. Tanzella and R.D. Weaver, 176th Meeting of the Electrochemical Society, Hollywood, FL, October 1989.

V.C. Noninski and C.I. Noninski, 176th Meeting of the Electrochemical Society, Hollywood, FL, October 1989.

K.S.V. Santhanam, J. Rangarajan, O'N. Braganza, S.K. Haram, N.M. Limage and K.C. Mandal, Indian J. Technol., 27 (1989) 175.

11. R. Adzic and E. Yeager, Case Center for Electrochemical Science Annual Conference, 30-31 October 1989, Cleveland, OH; to be published.
12. R.A. Oriani, J.C. Nelson, S.K. Lee and J.H. Broadhurst, 176th Meeting of the Electrochemical Society, Hollywood, FL, October 1989; Nature, submitted.
13. N. Lewis, 175th Meeting of the Electrochemical Society, Los Angeles, CA, May 1989.
14. N. Lewis, M.J. Heben, A. Kumar, S.R. Lunt, G.E. McManis, G.M. Miskelly, R.M. Penner, M.J. Sailor, P.G. Santangelo, G.A. Shreve, B.J. Tufts, M.G. Youngquist, C.A. Barnes, R.W. Kavanagh, S.E. Kellog, R.B. Vogelaar, T.R. Wang, R. Kondrat and R. New, Nature, 340 (1989) 525.
15. D.E. Williams, D.J.S. Findlay, D.H. Craston, MR. Sen6, M. Bailey, S. Croft, B.W. Hooten, C.P. Jones, A.R.J. Kucernak, J.A. Mason and R.I. Taylor, Nature, 342 (1989) 375.
16. R.G. Keesing, R.C. Greenhow, M.D. Cohler and A.J. McQuillan, Nuovo Cimenta, submitted. M. Chemla, J. Chevalet, R. Bury and M. Perie, Cold Fusion Session, 40th Meeting of the International Society of Electrochemistry, Kyoto, 11-18 September 1989.

G. Kreysa, M. Schtitze, G. Marx, W. Plieth, B. Zeitnitz, W. Heeringa and H.O. Klages, Cold Fusion Session, 40th Meeting of the International Society of Electrochemistry, Kyoto, 11-18 September 1989.

A. Bruggeman, M. Loos, C. Van der Poorten, R. Craps, R. Leysen, F. Poortmans, G. Verstappen and M. Snykers, Studiecentrum voor Kernenergie Report, September 1989.

M.E. Hayden, U. Ndrger, JL. Booth, L.A. Whitehead, W.N. Hardy, J.F. Carolan, E.H. Wishnow, D.A. Balzarini, J.H. Brewer and C.C. Blake, submitted.

J.P. Blaser, 0. Haas, C. Petitjeau, C. Barbero, W. Bertl, K. Lou, M. Mathias, P. Baumann, H. Daniel, J. Hartmann, E. Hechtl, P. Ackerbauer, P. Kammel, A. Scrinzi, H. Zmeskal, T. Kozlowski, R. Kipfer, H. Baur, P. Signer and R. Wieler, Chimia, submitted.

R. Behrisch, W. Moller, J. Roth and B.M.V. Scherzer, Nucl. Fusion, 29 (1989) 1187.

H.S. Bosch, G.A. Wurden, J. Gernhardt, F. Karger and J. Perchermeier, Report IPP 111/149' of the Max-Planck Institut fur Plasmaphysik, Garching bei Munchen.

V. Eberhard, G. Fieg, K. Flory, W. Heeringa, H.V. Karow, H.O. Klages, J. Lebkucher, M. Moschke, C. Politis, J. Romer, H. Schnider, G. Volker, H. Werle, H. Wiurtz and B. Zeitnitz, Report INR-1653 of the Kernforschungszentrum Karlsruhe, 1989.

17. R.D. Armstrong, Cold Fusion Session, 40th Meeting of the International Society of Electrochemistry, Kyoto, 11-18 September 1989.
18. R.D. Armstrong, E.A. Charles, 1. Fells, L. Molyneux and M. Todd, Electrochim. Acta, 34 (1989) 1319.
19. To be published.
20. G.M. Miskelly, M.J. Heben, A. Kumar, R.M. Penner, M.J. Sailor and N.S. Lewis, Science 246 (1989) 793.
21. R. Garwin, Nature, 338 (1989) 616.
22. V.J. Cunnane, R.A. Scannei and D.J. Schiffrin, J. Electroanal. Chem., 269 (1989) 437.
23. G. Kreysa, G. Marx and W. Plieth, J. Electroanal. Chem., 266 (1989) 437.
24. M.E. Wadsworth, S. Guruswamy, J.G. Byrne and J. Li, to be published.
25. J. Vöelkl and G. Alefeld (Eds.), Hydrogen and Metals, Vol. 2, in Topics in Applied Physics, Vol. 29, Springer Verlag, Berlin, 1978, Ch. 12.
26. E. Teller, National Science Foundation - Electric Power Research Institute Meeting, Washington, DC, 16-18 October 1989.
27. P.I. Dee, Nature, 133 (1934) 564.
28. P.I. Dee, Proc. R. Soc. A, 148 (1935) 623.
29. W.B. Ard, M.L. Becker, R.A. Dandl, H.O. Eason, A.C. England and R.J. Kerr, Phys. Rev. Lett., 10 (1963) 87.